Deep learning-aided analysis of 3D cell culture microscopic images to enhance the precision of the drug screening process : A use case for cervical cancer

Tarek Maylaa

Ecole doctorale Science de l'ingénierie et des systèmes (ENGSYS-632)

IEMN - Institut d'électronique de microélectronique et de nanotechnologie

Thèse présentée par

TAREK MAYLAA

En vue de l'obtention du grade de

Docteur de l'Université de Lille

Spécialité: Electronique, microélectronique, nanoélectronique et micro-ondes

Analyse d'images microscopiques de culture cellulaire 3D assistée par apprentissage en profondeur pour améliorer la précision du processus de dépistage des médicaments : un cas d'utilisation pour le cancer du col de l'utérus

Présentée et soutenue publiquement le 19 Janvier 2023

Membres du jury:

Rapporteurs	M. Cosimo DISTANTE	Professeur, University of Salento
	M. Yassine RUICHEK	Professeur, Université de Technologie de Belfort Montbéliard
Président	M. Abdelmalik TALEB-AHMED	Professeur, Université Polytechnique Hauts-de-France
Examinatrices	Mme Alice OTHMANI	MCF, HDR, Université Paris-Est Créteil
	Mme Rim SALMI SLAMA	Ph.D, Enseignante-Chercheuse, Cesi Lyon
Directeur de thèse	M. Dominique COLLARD	DR CNRS, Université de Lille
Encadrants	Mme Feryal WINDAL	Ph.D, Enseignante-chercheuse, Junia ISEN Lille
	M. Halim BENHABILES	Ph.D, Enseignant-chercheur, Junia ISEN Lille
Invités	Mme Nathalie MAUBON	Ph.D, PDG, HCS Pharma
	M. Gregory MAUBON	Ph.D, Directeur du Digital, HCS Pharma

The Graduate School ENGineering and SYstem Sciences (ENGSYS-632)

IEMN - Institute of Electronics, Microelectronics and Nanotechnology

Thesis submitted by

TAREK MAYLAA

In order to obtain the grade of

Doctor from the University of Lille

Specialty: Electronics, microelectronics, nanoelectronics and microwaves

Deep learning-aided analysis of 3D cell culture microscopic images to enhance the precision of the drug screening process: A use case for cervical cancer

Presented et publicly defended on the 19th of January 2023

Member of the jury:

Reviewers	M. Cosimo DISTANTE	Professeur, University of Salento
	M. Yassine RUICHEK	Professeur, Université de Technologie de Belfort Montbéliard
President	M. Abdelmalik TALEB-AHMED	Professeur, Université Polytechnique Hauts-de-France
Examiners	Mme Alice OTHMANI	MCF, HDR, Université Paris-Est Créteil
	Mme Rim SALMI SLAMA	Ph.D, Enseignante-Chercheuse, Cesi Lyon
Thesis Director	M. Dominique COLLARD	DR CNRS, Université de Lille
Thesis Supervisors	Mme Feryal WINDAL	Ph.D, Enseignante-chercheuse, Junia ISEN Lille
	M. Halim BENHABILES	Ph.D, Enseignant-chercheur, Junia ISEN Lille
Invitees	Mme Nathalie MAUBON	Ph.D, CEO, HCS Pharma
	M. Gregory MAUBON	Ph.D, CDO, HCS Pharma

Declaration of Authorship

I, Tarek MAYLAA, declare that this thesis titled, "Deep learning-aided analysis of 3D cell culture microscopic images to enhance the precision of the drug screening process: A use case for cervical cancer" and the work presented in it are my own. I confirm that:

- This work was done wholly or mainly while in candidature for a research degree at this University.
- Where any part of this thesis has previously been submitted for a degree or any other qualification at this University or any other institution, this has been clearly stated.
- Where I have consulted the published work of others, this is always clearly attributed.
- Where I have quoted from the work of others, the source is always given. With the exception of such quotations, this thesis is entirely my own work.
- I have acknowledged all main sources of help.
- Where the thesis is based on work done by myself jointly with others, I have made clear exactly what was done by others and what I have contributed myself.

Signed:

_____

Date:

_____

"Artificial intelligence is the future and the future is here."

Dave Waters

UNIVERSITÉ DE LILLE

Abstract

Faculty of Science and Technology

BioMEMS Group

Deep learning-aided analysis of 3D cell culture microscopic images to enhance the precision of the drug screening process: A use case for cervical cancer

by Tarek MAYLAA

With the lack of efficient medicine to treat cancer, there is a need to improve the drug discovery process. To this extent, the use of cell culture methods has been privileged for drug testing. 2D cell cultures were widely favored for their low cost and low complexity however several limits forced the scientific community to provide 3D cell culture methods. However, the microscopic images acquired from the 3D cell culture becomes more challenging because of their complexity. In this thesis, we develop automatic methods for processing microscopic images from these 3D cell cultures. We first tackle the nuclei segmentation problem that is a crucial part in the analysis of these images. Our study consists of preparing a benchmark for the evaluation of machine learning methods. We have thus compared the performances of several classifiers that were trained for the segmentation of nuclei. This allowed us to conclude that these methods still struggle in separating effectively the nuclei inside a z-stack images. To respond to this problematic, we developed a deep learning workflow that first detect the spheroids inside the images and then segment the nuclei inside each spheroid. Deep learning architectures provided good performances which contributed to the 3D reconstruction of the nuclei. This work provides an additional help for the biologists in their analysis.

UNIVERSITÉ DE LILLE

Résumé

Faculté des Sciences et Technologies

Groupe BioMEMS

Analyse d'images microscopiques de culture cellulaire 3D assistée par apprentissage en profondeur pour améliorer la précision du processus de dépistage des médicaments : un cas d'utilisation pour le cancer du col de l'utérus

de Tarek MAYLAA

Avec le manque de moyens efficaces pour lutter contre le cancer, il est nécessaire d'améliorer le processus de découverte de médicaments. Dans cette mesure, l'utilisation de méthodes de culture cellulaire a été privilégiée. Les cultures cellulaires 2D ont été largement utilisées pour leur abordabilité et leur faible complexité, mais plusieurs limites ont obligé la communauté scientifique à fournir des méthodes de culture cellulaire 3D plus proches du caractère humain. Cependant, les images microscopiques acquises à partir de la culture cellulaire 3D deviennent plus difficiles à interpréter à cause de leur complexité. Dans cette thèse, nous développons des méthodes automatiques de traitement d'images microscopiques issues de ces cultures cellulaires 3D. Dans un premier temps, nous abordons le problème de la segmentation des noyaux qui est un élément crucial dans l'analyse de ces images. Pour se faire, notre étude consiste à préparer un benchmark pour l'évaluation de méthodes d'apprentissage automatique. Nous avons ainsi comparé les performances de plusieurs classifieurs entraînés pour la segmentation des noyaux. Ceci nous a permis de conclure que ces techniques n'arrivent pas à séparer efficacement les noyaux dans un z-stack. Pour répondre à cette problématique, nous avons également développé une chaîne de traitements basée sur l'apprentissage profond qui détecte d'abord les sphéroïdes à l'intérieur des images, puis segmente les noyaux à l'intérieur de chaque sphéroïde. Ces architectures d'apprentissage profond ont fourni de bonnes performances qui ont contribué à la reconstruction 3D des noyaux. Ce travail est considéré comme une aide supplémentaire aux biologistes pour mener leurs analyses.

Acknowledgements

First of all, I would like to thank my supervisors Dr. Halim Benhabiles and Dr. Feryal Windal who were always present during these 3 years and were a source of motivation with their daily encouragements. I really appreciated working with them as they introduced me to the scientific research in artificial intelligence and helped me achieve daily progress. I would also like to thank my thesis director Pr. Dominique Collard who followed me during this time and gave me helpful recommendations to guide me towards success.

In addition, I send my deepest gratitude to the HCS Pharma team, in particular to Dr. Nathalie Maubon, Dr. Gregory Maubon and Dr. Elodie Vandenhaute for providing us with the data that contributed in the progress of this work. They also dedicated their time in the annotation process for the images and were always present to ensure the advancement of this study.

Special thanks goes to the members of the Digital Systems and Health Sciences department at Junia as they provided us with all the materials and equipments that we need.

Another big thank you goes to Theo Delobelle, Thomas Dumont and Romain Vanhee who are currently graduates at ISEN Junia Lille. I was their tutor in an M2 project and with their motivation, dedication and great help we developed the workflow of the nuclei clustering and 3D reconstruction.

I would also like to send my appreciations to my previous mentors and advisors at the American University of Science and Technology in Beirut, in particular to Dr. Roger Achkar, Mr. Michel Owayjan, Dr. Hiba Othman, Dr. Hoda Mokbel and Mr. Elie Abdo. I consider myself lucky to be mentored by them as I learned a lot from them during my bachelor and masters programs.

I want to thank also my friends Elie, Bilel, Hakim, Mia, Marco, Charbel, Roula, Luis, Marc, Joe, Ismaeil, Ali, Dany, Ghinwa and my colleagues Ziheng and Ruiwen who lives in France or abroad for their constant care and support.

Last by not least, I want to thank my family who although lives far away was always present to encourage me through every step and difficult moments.

Contents

List of Figures

List of Tables

List of Abbreviations

HCS	**H**igh**C**ontent **S**creening
Weka	**W**aikato **E**nvironment for **K**nowledge **A**nalysis
RF	**R**andom **F**orest
MLP	**M**ulti **L**ayer **P**erceptron
ANN	**A**rtificial **N**eural **N**etwork
MO	**M**ean **O**verlap
UO	**U**nion **O**verlap
IOU	**I**ntersection **O**ver **U**nion
YOLO	**Y**ou **O**nly **L**ook **O**nce
MSC	**M**ean **S**hift **C**lustering
DBSCAN	**D**ensity-**B**ased **S**spatial **C**lustering of **A**pplications with **N**oise

Dedicated to Lebanon and its people who are going through difficult times.

Chapter 1

Introduction

1.1 Context

Our society faces one of the most important challenges in our history in terms of public health: cancer. It is a disease defined by an abnormal growth of cells that can spread through the entire body. After heart disease, cancer is the second leading cause of death worldwide that killed approximately 9,6 million people until 2018. According to the Centers for Disease Control and Prevention (CDC), 1 752 735 new cancer cases emerged in the United States leading to 599589 deaths in 2019 [17]. Cancer is considered one of the main causes of death among women worldwide. Women represents 49.5% of the population and form a much larger percentage of the population over 60 years. Cancer is considered the second leading of death of women in America and Europe. There is an estimation of 6,7 million new cancer cases and 3.5million deaths among females in 2012 [73]. Figure 1.1 represents the incidence and mortality rates of all cancer among women worldwide.

Cervical cancer is the fourth most common cause of cancer in women after breast, colorectal, and lung cancer worldwide [4]. In 2018, around 570 000 women were diagnosed with the disease, eventually leading to 311 000 deaths from the disease worldwide. American cancer society have an estimation of 14 100 cases of invasive cervical cancer with a death toll reaching approximatively 4 800 among women in the United States for 2022 [18]. Here comes the need to develop and discover more drugs and medicinal procedures for cancer treatments. Nowadays several treatments such as immunotherapy and cytotoxic chemotherapy are available to stop the spread of the disease. However, these treatments often have side effects that can be

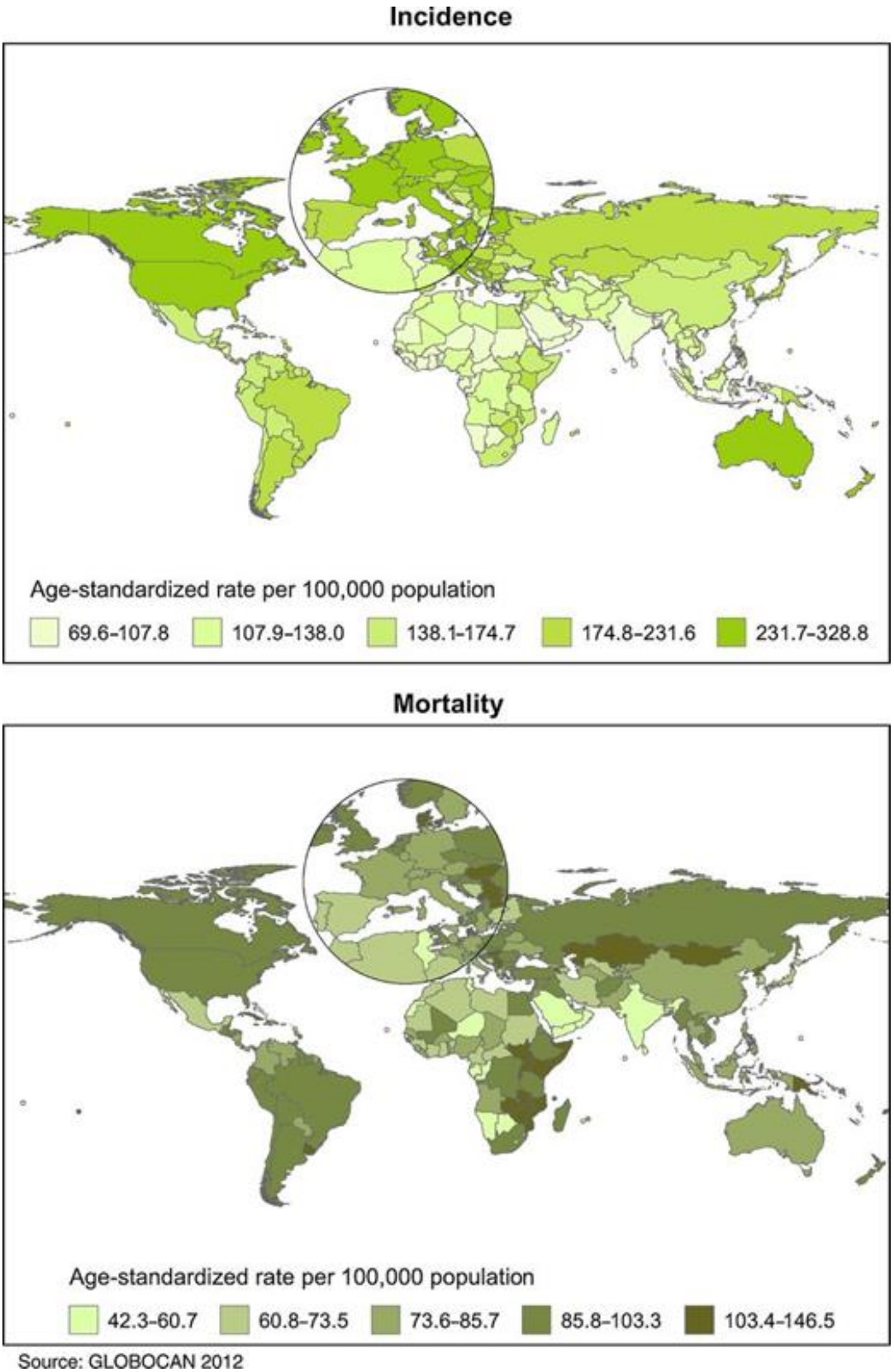

FIGURE 1.1: World map of cancer incidence and mortality rates among women

either acute or permanent. Common acute reactions from cytotoxic chemotherapy include skin reactions, alopecia, anemia, as well as renal, cardiovascular, and neurological impairment. Severe reactions may include paralysis, spasms, and coma. Also, infertility is a common chronic side effect [66]. Figure 1.2 [21] represents the cervix organ and the localisation of the cervical cancer. This highlights the need to develop more effective and less toxic pharmacological treatments for cervical cancer. However, drug development is expensive. The cost for the development of a single drug can range **from 161 million to 1,8 billion United States dollars**. According to the Food and Drug Association (FDA) of the United States, the drug development process typically involves five stages: early drug discovery, pre-clinical research, clinical research, pre-commercialization drug FDA review, and post-market drug safety monitoring by the FDA [24]. As a result, the drug development process is expensive and can take up to 12 years [56], highlighting the need to develop techniques to speed up the process without compromising on safety. About two-thirds of potential beneficial drugs are rejected at the clinical research stage due to high toxicity levels (20%) or lack of efficiency (30%). The high failure rate at this stage further prolongs the drug development process. A key factor leading to a high failure rate at the preclinical stage is the difficulty to reproduce physiological conditions in-vitro, making it difficult to predict the efficacy and toxicity of the drug in-vivo.

In cellular in-vitro assays, two-dimensional (2D) monolayers of cells are generally used. Over the past decades, 2D cell cultures were used because they are easy to manipulate and cost-effective. This arrangement is completely different from the organization of cells in-vivo in the human body. It is now well established that three-dimensional (3D) cell cultures better mimic the structure and the behavior of human tissues [62] because they can take into account the interconnections between cells, the 3D structure of the tissues, and the extracellular matrix (ECM) surrounding the human cells (Figure 1.3). It should also be noted that 3D cellular models based on different cell culture systems without physical cell support (e.g., ultra-low attachment plate) or with different forms of cell supports (e.g., solids scaffold and hydrogels of different origins) are becoming more widely available. We can cite BIOMIMESYS® Hydroscaffold, a 3D cell culture technique developed by the compagny HCS Pharma based in France (Loos) and provides a physiological 3D

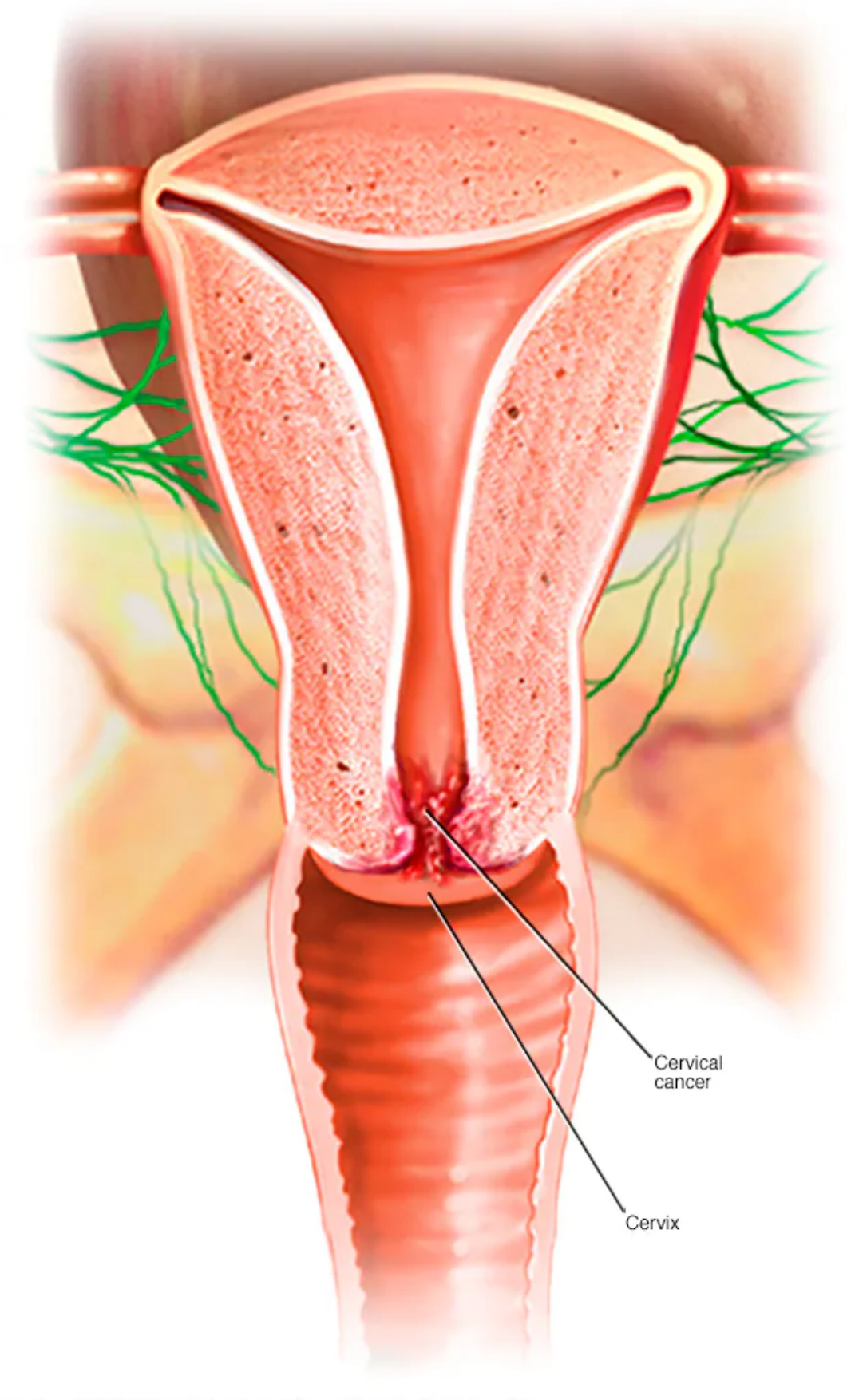

FIGURE 1.2: Cervical Cancer

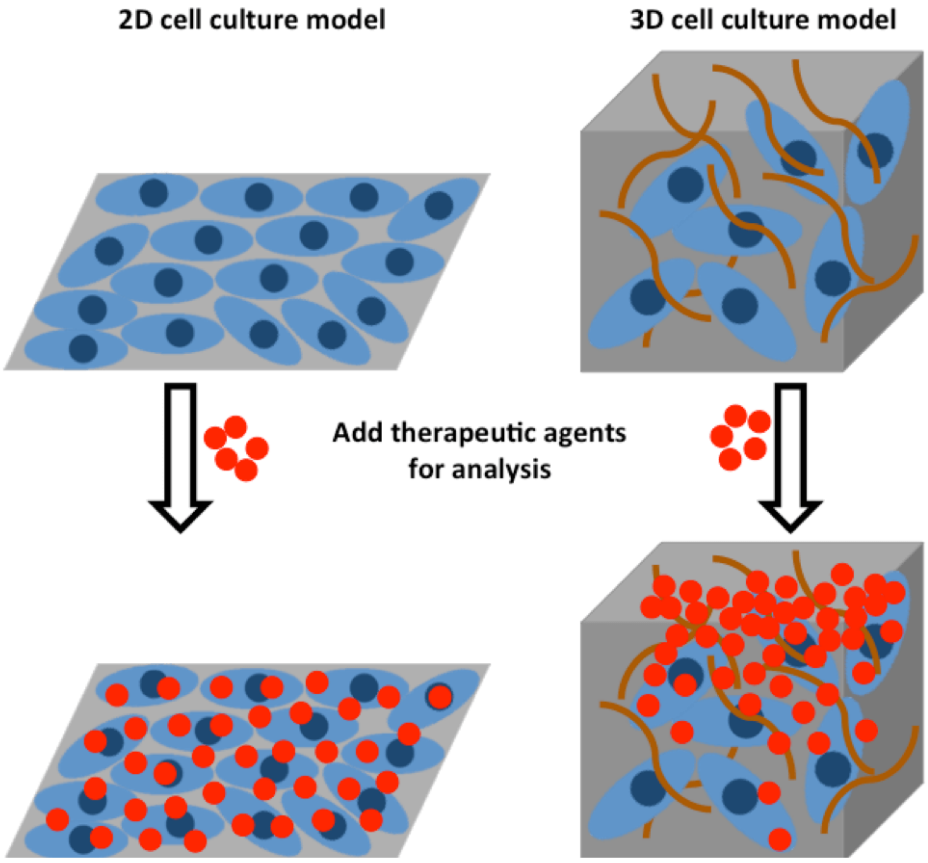

FIGURE 1.3: 2D vs 3D cell culture[1]

cell culture system. High content screening (HCS), also known as high throughput imaging, is essential for the development of new drugs [59]. This technique is based on fluorescence microscopy that is used to observe the cell structure on the microscopic images. It is a powerful tool as it allows to conduct a quantitative observation on the acquired images to analyse the occured changes. Fluorescence microscopy is based on fluorescence properties that molecules have. This means that they absorb the light at one wavelength and then reemit it at another wavelength. Therefore, fluorescent molecules (called fluorophores or fluorochromes) are able to interact with specific biological molecules of interest and are therefore often used to facilitate the visualization of cellular substructures.

Hoechst is a commonly used fluorochrome. This fluorescent molecule can penetrate the cell membrane and bind strongly to adenine–thymine-rich regions in DNA [49] and it can therefore be used to study the nuclei of cells. Molecular devices is an american supplier of bioanalytical systems that help in the drug discovery process.

FIGURE 1.4: MetaXpress prototype for High Content Screening**source**

They developped ImageXpress, an automated system for high content imaging acquisition [20]. Their system, shown in Figure 1.4, was used for microscopic images acquisition in our study.

However, the large number of images acquired during automated fluorescent microscopy makes the manual segmentation and analysis of subcellular components time-consuming for biologists. Furthermore, complex computational tools are required to evaluate the effects of treatment on cells from the images. Therefore accurate algorithms are required to facilitate the segmentation and analysis of cellular substructures on thousands of microscopic images [2]. Various machine learning algorithms using different architectures have been developed for this purpose. For example, The Waikato environment for knowledge analysis (WEKA) [38] provides a range of machine learning algorithms, image manipulation tools, and evaluation metrics for the segmentation of cell structures on microscopic images. Another commonly used tool is the Fiji (ImageJ) software [14], which provides a range of image

segmentation and imaging processing tools. These packages facilitate the development of segmentation tools for biologists with limited expertise in artificial intelligence.

1.2 Motivation and Contributions

Automatic tools are widely requested when it comes to microscopic images analysis. These demands are mainly focused on two reasons: first, the quantity of data images that we can acquire from the microscopy of cell culture. Indeed, we can obtain thousands of images taken from one plate of cell culture. This huge amount of data requires plenty of time to be treated manually while it can take minutes or even seconds using automatic tools. Second, the complexity of data can often be hard to be dealt manually. Working with dense cell environments or opaque mediums can often lead to several artifacts (blurred and overlapped spheroids and nuclei in Figure 1.5) in the images such as overlapping or blurred objects. This can affect the manual analysis as it can cause doubts and uncertainty among biologists and it can be hard to find and detect the main components inside the microscopic images. Working with cell culture and automatic tools to analyse the acquired microscopy images could lead to first accelerate the process of drug discovery since it is an automated process that can analyse thousands of images and giving lots of results in a short time. It also reduces animal testing as we are working in 3D cell culture environment that mimics the cellular components and behavior inside the human body.

As stated above, various tools are available to perfom automatic analysis. These tools are powerful enough to assist biologists and non-specialists in artificial intelligence. As our images are acquired from 3D cell culture, they are represented in z-stacks of 2D images so that each stack can form the 3D representation of the environment after reconstruction (Figure 1.5). Thus we are faced with major questions in the air of image analysis: to what extent the automatic tools could still provide an efficient and robust analysis regarding microscopic images from 2D vs 3D cell cultures ? Would these methods perform well on our z-stack images ? And most importantly,

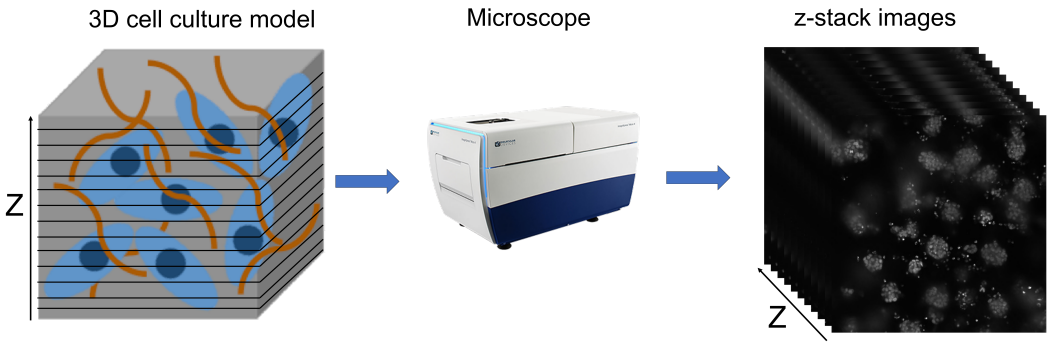

FIGURE 1.5: z-stack images from 3D cell culture microscopy

could deeper automatic techniques contribute in the progress of microscopic analysis thus assisting the scientific community to accelerate the process of drug screening ? To this extent we proposed two different contributions. The first one is a quantitative and qualitative evaluation of several built-in segmentation methods through the Fiji and WEKA softwares to evaluate the efficiency of these tools on our composed dataset. The second one is a workflow process based on deep learning and machine learning algorithms that first detect the spheroids and segment the nuclei inside each spheroid thus helping us achieve a 3D reconstruction of the nuclei.

A benchmark for the evaluation of segmentation methods– Our first contribution is the proposition of a benchmark for the evaluation of nuclei segmentation. Detecting the nuclei in the microscopic images is an essential task for biologists since they get multiple morphological and physiological information from a nucleus after a drug interaction. Our benchmark is composed of a dataset of microscopic images, a set of ground truth and two different similarity metrics. The microscopic images acquired at HCS Pharma from 3D cell culture of HeLa cells (cervical cancer cells) [39] were manually annotated by three different biologists and experts. We based the evaluation on different machine learning built-in classifiers, in image processing and data analysis tools (Fiji and WEKA) that are widely used by biologists, for the purpose to segment the nuclei in the microscopic images and find the best method that can help the experts in their work. We used also some image processing and manipulation techniques to enhance the obtained results. To assess the quantitative

evaluation, the metrics measured the comparison between the obtained segmentation result with the manually segmented one thus giving us a similarity rate. We propose a detailed study on exisiting built-in classifiers and try to improve the performance by applying image processing methods such as majority voting methods that combines the results obtained from different models. Then we evaluate these performances with the similarity metrics and assess the robustness of such methods by testing them first on different 2D images in the same z-stack and second on other microscopic images acquired from different datasets. We show that while these methods are efficient for certain tasks they still have limits with images that contains artefcats such as blurriness and overlapping objects. This work contributed in a paper entitled "An Evaluation of Computational Learning-based Methods for the Segmen-tation of Nuclei in Cervical Cancer Cells from Microscopic Images" and was published in the Current Computer Aided Drug Design journal from Bentham Science Publisher.

A workflow based on deep learning and machine learning methods to achieve the 3D reconstruction of the nuclei– As we deducted in the first contribution, there is a need to develop robust and efficient automatic tools to study, evaluate and help in the analysis and interpretation of microscopic images acquired from 3D cell culture. Indeed, the complexity of these type of images prevent the biologists to be able to perform manual and visual interpretation as the complexity is present in form of the amount of the data that need to be analysed and the translucent environment that affects the images with some artifacts. This is why biologists need automatic tools that can help in the analysis by first detecting the important components in the images and then perform the 3D reconstruction and thus allowing the biologists to conduct a robust analysis on the cellular components (nuclei, cells, etc.). To answer to this problematic, we proposed a workflow based on learning processes to first detect the spheroids inside the microscopic stack images, then to segment the nuclei inside each spheroid thus being able to reconstruct the segmented nuclei in the stack and obtain the 3D reconstruction. The spheroid detection analysis and the segmentation analysis were based on deep learning methods. They succeeded in first detecting the spheroids inside each image in the stack and the segmentation

process actually outperformed the manual segmentation that was conducted by human observers. As for the 3D reconstruction, we performed a qualitative evaluation of two machine learning clustering methods to track each segmented nucleus in all the stack and thus apply a mesh reconstruction to have the 3D representation. The outcome of this work was a paper entitled "A hierarchical deep learning framework for nuclei 3D reconstruction from microscopic stack-images of 3D cancer cell culture" and was presented in the 6th World Conference on Smart Trends in Systems, Security, and Sustainability and published in Springer LNNS.

1.3 Thesis Organization

As this manuscript describes and recounts the 3 years that were dedicated on this project, it is devided into four more chapters:

Chapter 2 talks about the biological aspect of this project. As cell culture and microscopy are two major assets in this work, it was important to understand some scientific information and functionalities in the biopharmaceutical field. Indeed this chapter will start by introducing the importance of cell culture in drug discovery and how it will help in finding treatments to benign and malignant tumors. Furthermore, the history of drug discovery and drug screening and the different discovered treatments for cancer are also developed. Likewise, in this chapter, we defined the cell culture process linking it to the culture of cancerous cells while giving the difference between 2D and 3D cell culture. We also highlight the importance of cell culture regarding drug discovery and will give a reminder of the drug screening process. In addition, this chapter will focus on the microscopy process and the different parameters that affects the generated images. It will also introduce high content screening and its importance in such work.

Chapter 3 presents our benchmark for the evaluation of the segmentation results obtained through different built-in classifiers. This chapter starts by indicating the motivation behind this work while presenting the different scientific studies that dealt with nuclei segmentation. It then introduces the generated dataset and the methods used for the experimentation. Subsequently, it details the experimentation

process by describing each step from the training process to the quantitative and qualitative evaluations.

Chapter 4 presents the learning based workflow for the 3D reconstruction of the nuclei. The chapter starts with an introduction that motivates such work by displaying the fact that existing methods suffer to perform well with complex images that contains several artefcats. It then goes by describing the workflow process and all the steps needed to achieve the 3D reconstruction goal. It continues by thouroughly explaining all the experimentations and results obtained to conclude with the final 3D reconstructed result.

Chapter 5 concludes the 3 years of work by summarizing the work that has been done and highlighting the contributions that we provided. Furthermore, it will end by giving some perspectives and ideas that can be subjects for future research projects to be added to this study.

Chapter 2

Cell culture and Microscopy for the Drug Screening Analysis

2.1 Introduction

Drug discovery is a significant process in medicine. It allows the development of new treatments for different conditions, diseases and even tumors. Drug discovery became a crucial task in the pharmaceutical industry and its progress is very beneficial to treat and maybe eradicate deadly tumors such as cancer. Cancer is considered a benign or malignant tumor that is defined by an abnormal and uncontrollable growth of body cells in any part in the body.

To be able to detect, follow the proliferation and progress of the cancer, in vitro cell culture is found to be efficient. In vitro cell culture is defined by the extraction of cells from a human, animal or plant body and the observation of the growth of these cells in an artificial environment [42]. Cell culture also proved to be an asset for drug discovery, where several drugs are tested in the cell culture environment and biologists are able to observe the changes and transformations that follow through optical microscopy. One type of optical microscopy is fluorescence microscopy, a technique that is important in biomedical science. Fluorescence microscopy is the principle of irradiation of UV light to certain structures inside the cell that in turn emits light and thus appearing on the image. To be able to show specific components from the cell environment, there is a variety of fluorescent stains that can be used [28]. For example the DAPI stain [25] is a fluorescent stain that is used for nuclei staining. Confocal fluorescence microscopy technique generated images with higher resolution using a

confocal microscope. It is generally used to provide three-dimensional microscopic images [28].

Over the years, scientists developed different microscopy methods to help them achieve their analysis. From these methods we can cite, High-content screening (HCS) [40], a method that combines automatic imaging with quantitative data analysis and thus being able to evaluate directly and automatically the images that are acquired. HCS uses automated fluorescence microscopy to acquire images of the internal cell structures. These images are then used to quantify the cellular changes among a single or population of cells while undergoing pharmaceutical treatments. These changes are then analyzed [50] to evaluate the treatment's efficacy and/or toxicity.

As high content screening are widely used, the need to develop efficient automatic method became also highly demanded. Indeed, as these methods can produce a significant amount of microscopic images in a short amount of time, biologists alone are not able to analyse them manually. Moreover, automatic methods that serve different tasks such as localizing cancerous cells or nuclei, segmenting the different cell structures in the image, giving measurements or indication of occurred changes can meaningfully assist in the progress of drug discovery process.

2.2 Drug discovery and cancer treatments

2.2.1 Drug discovery

Drug discovery is the process of developing drugs and treatments to help eradicate or stop the spreading of benign or malignant diseases and tumors. It is an important process in the pharmaceutical industry and has lead to new opportunities and scientific progress in medicine. However, drug discovery is time consuming and expensive. Indeed, it can take up to 12 years and between **$314 million to $2.8 billion to develop a certain drug [81]**. According to the U.S. Food and Drug Administration (FDA), the drug discovery process is divided into 5 stages (Figure 2.1) [24]:

Discovery and Development– This is the first stage of drug discovery. It consists of identifying and understanding a certain disease and start testing thousands of

chemical compounds to find suitable candidates. It is crucial afterwards to gather information from the few candidates left to determine several criterias such as the benefits of the drug, its best dosage, its side effects and its reaction with other treatments.

Preclinical Research– The second stage of drug discovery consists of measuring the toxicity of the drug candidate. it indicates the level of harmness that the drug may cause. This stage can generally take up to 6 years to give detailed analysis on dosing and toxicity pourcentage.

Clinical Research– The clinical research or clinical trials stage consists of understanding the effect of the candidate drugs on the human body. To this extent, the drug candidate is tested on a group of people that are selected based on several criterias. This stage is divided into 4 phases. In each phase the number of participants increases to be able to gather as much data on the efficacity of the drug. Each phase can take up to 7 to 12 months with the last phase going up to 4 years.

FDA Drug Review– This fourth stage is basically the thorough examination of the FDA professional team on the submitted drug. They check all the submitted data and facts to decide if the drug is safe for marketing.

FDA Post-Market Safety Monitoring– To confirm the safety of the drug over several years of market usage, the FDA monitors and reports the cases to put some limitations or regulate the dosage if needed.

2.2.2 Cancer treatments and side effects

As we can deduce, drug discovery is indeed time consuming. This is problematic when dealing with malignant tumors as people are in danger and the ratio of the number of death to the number of cases is particularly high.Taking cancerous tumors

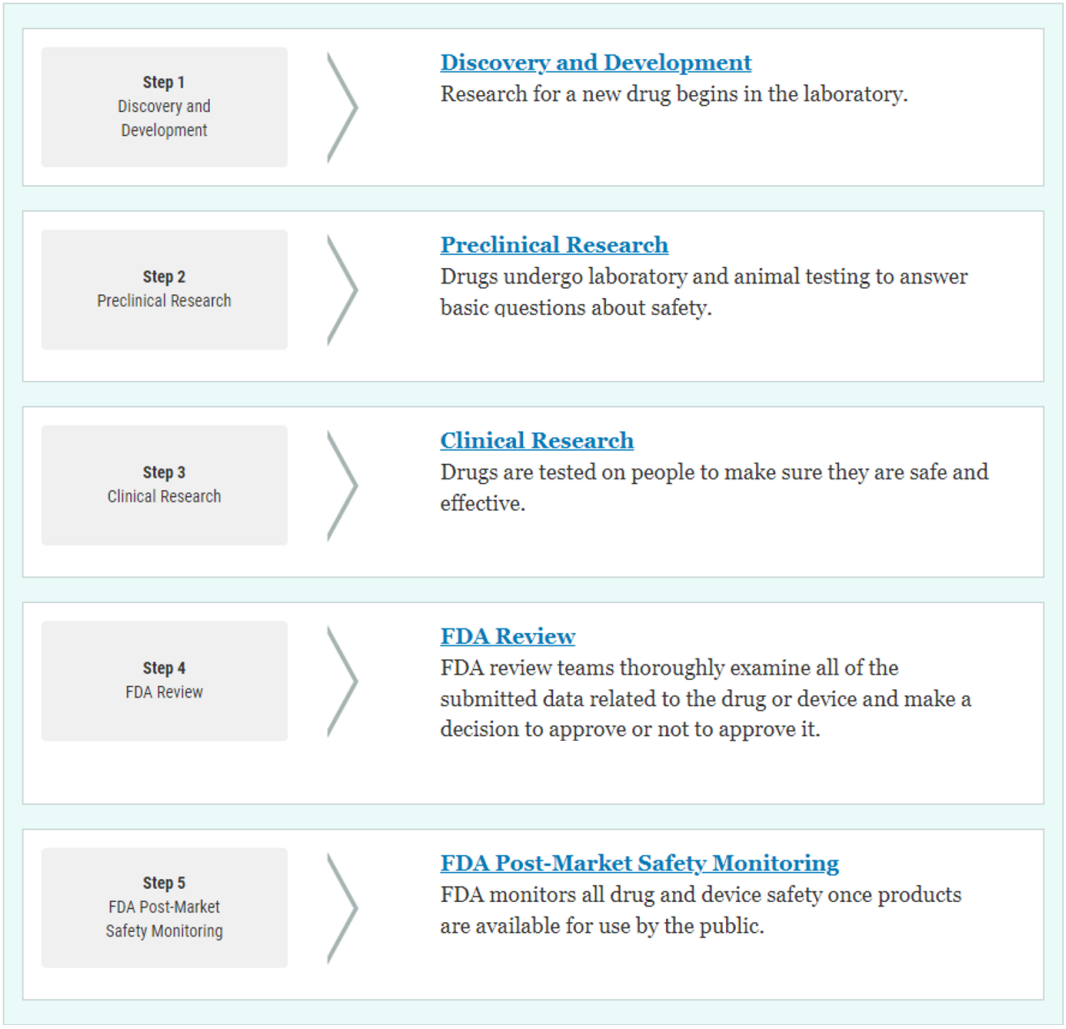

FIGURE 2.1: The drug development process implemented by the FDA

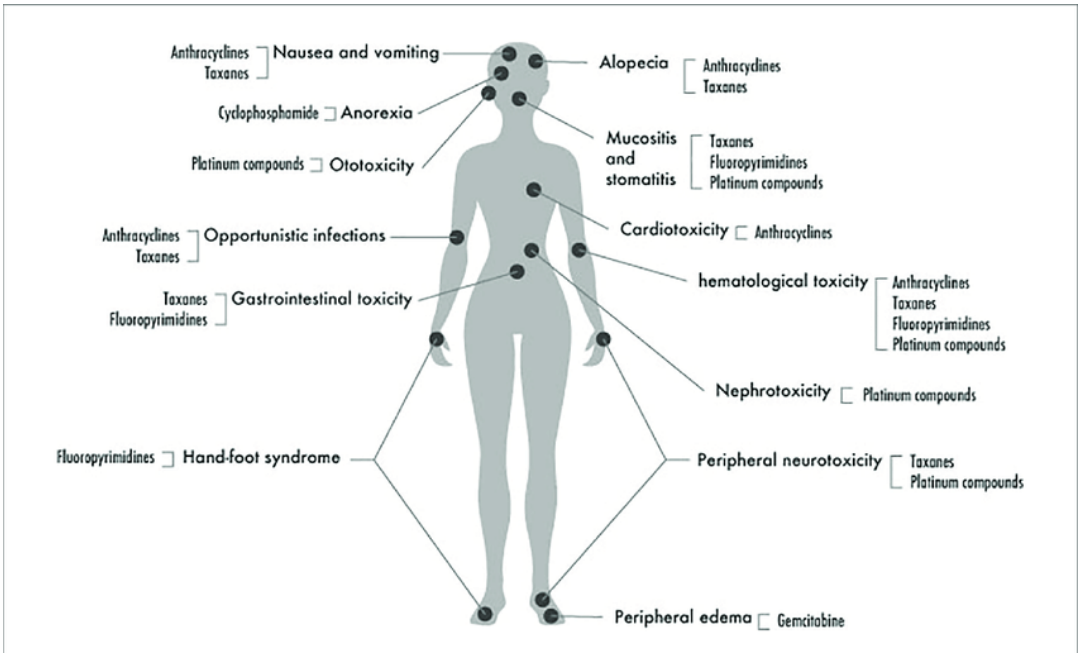

FIGURE 2.2: Side effects of chemotherapy [54]

as our reference, there were around 10 million deaths worldwide in 2020 [32] . Different treatments for cancer such as chemotherapy, radiation therapy, immunotherapy,etc. are widely used to help stop the spreading of the disease. However, the side effects of such treatments are likely to be serious. The world health organization classed these side effects into grades going form 0 to 4 [66]. Grade 1 is considered mild as grade 2 represents moderate reactions. Grade 3 and 4 are considered severe and life threatening. The reactions of these treatments can be seen on different part of the body such as skin, hair and blood. In addition, body organs can also be affected such as the heart, lungs, kidneys and brain. When dealing with grade 3 and 4 effects, it may cause neurotoxicity that can develop paralysis and even lead to coma (Figure 2.2).

2.2.3 Cervical cancer

Cervical cancer is a deadly tumor among women. In 2012, 266 000 women died among 528 000 recorded cases worldwide [77]. This increased in 2018 as 311 000 deaths occured [4]. The lead cause of cervical cancer development is human papillomavirus (HPV). HPV is the most common transmittable sexual disease worldwide. If HPV infection persists and is not treated, it can lead to a cancerous tumor around 10 years later thus resulting in cervical cancer among women [6].

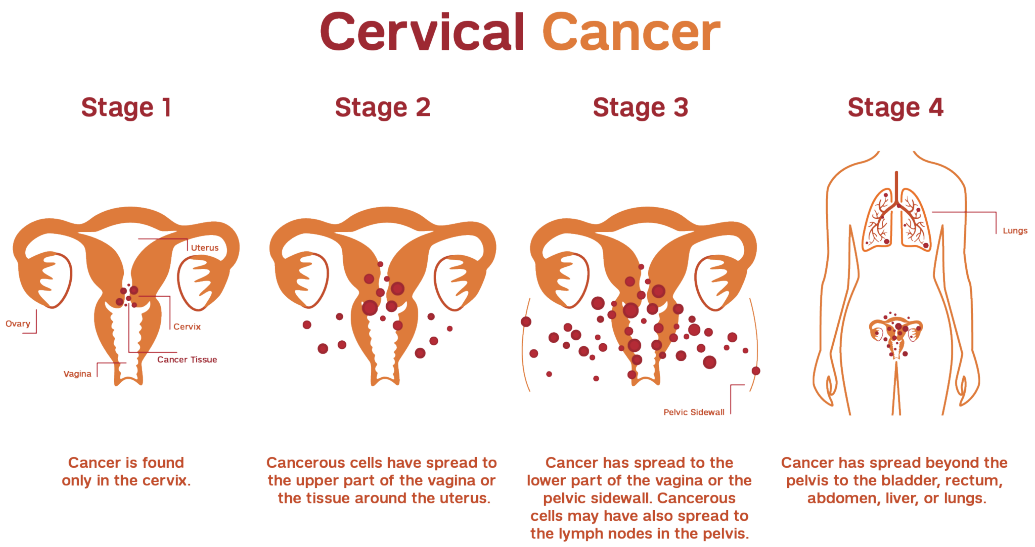

FIGURE 2.3: The different stages of cervical cancer [22]

Once a cervical cancer diagnosis is given, a stage is attributed to the patient. It is determined by the size of the tumor and its spreading of it around the cervix [78]. Stages varies from 1 to 4 based on the seriousness of the tumor. Stage 1 signifies that the tumor is located in the cervix region and did not spread. Stage 2 and 3 are identified when the tumor goes beyond the cervix and into the pelvis but is still contained. Stage 4 is critical since it indicates that the tumor goes way beyond the cervix and started affecting other organs. Survival rate of stage 4 cervical cancer is considered low (Figure 2.3). According to the American cancer society, the 5 year survival rate drops from 92% for stage 1 patients to only 18% for patients with stage 4 cervical cancer [23]. Usually patients with stage 4 cervical cancer undergo treatments such as radiation therapy and chemotherapy, however and as stated before, these treatments have significant side effects that may be harmful. There is a scientific urge to develop effective methods that help accelerate the drug discovery and drug testing procedures to first, be able to raise the survival rate for patients with malignant cancer and second, treat patients with at least harmless side effects on their physical and mental states.

2.3 2D vs 3D Cell Culture

Cell culture is an in vitro process of growing cells in an artificial environment. Cell culture became a crucial part of the drug discovery process as animal testing is being condemned internationally. The three Rs principle was introduced in the 1960s. It refers to the Replacement, Reduction and Refinement for the welfare of the animals [35]. Replacement means to establish alternative methods to animal testing. These methods can be both abosulte replacements as having computational models and using cell culture or relative methods as invertebrates that have lower pain sensitivity. Reduction stands for finding strategies to reduce the amount of animals that are exploited. Last but not least, Refinement indicates to develop new procedures that are not harmful to species. 2D cell culture is widely used due to its simplicity and low cost to maintain [45]. However, this method does not fully represent the tumoral cells behavior. Indeed, it does not fully mimic the cell-to-cell and cell-to-extracelular interactions that are responsible for the cell differentiation, proliferation as well as other functions [62] [7]. Moreover, morphological changes are noticed when the cells are transferred to the in-vitro culture. These alterations can affect the cell structure and secretion [27]. In addition, tumorous cells in-vitro have access to unlimited ressources such as oxygen and nutrients which is not the case in-vivo where the availability of such ressources depends on the size of the tumor [62].

To this extent, scientists became progressively more attracted to the development of 3D cell cultures since they believe it could give a better precision and thus contribute in a significant progress in drug discovery. In a 3D cell culture, all the mentionned limits such as the cell morphological and physiological changes, the cell-to-cell and the cell-to-extracelular interactions as well as the amount of oxygen and nutrients are resolved as it mimics the in-vivo conditions [48]. BIOMIMESYS® Hydroscaffold is an application of 3D cell culture provided by HCS Pharma located in Loos, France. BIOMIMESYS ensures a physiological 3D cell culture system based on a native ECM (hyaluronic acid, collagens, adhesion proteins, or peptides). This method combines the behavior of the solid scaffold with that of the hydrogel, eventually creating a relevant microenvironment for the 3D cell culture [9] in which the cancer cells usually grow as spheroids [12]. Figure 2.4 represents two microscopic

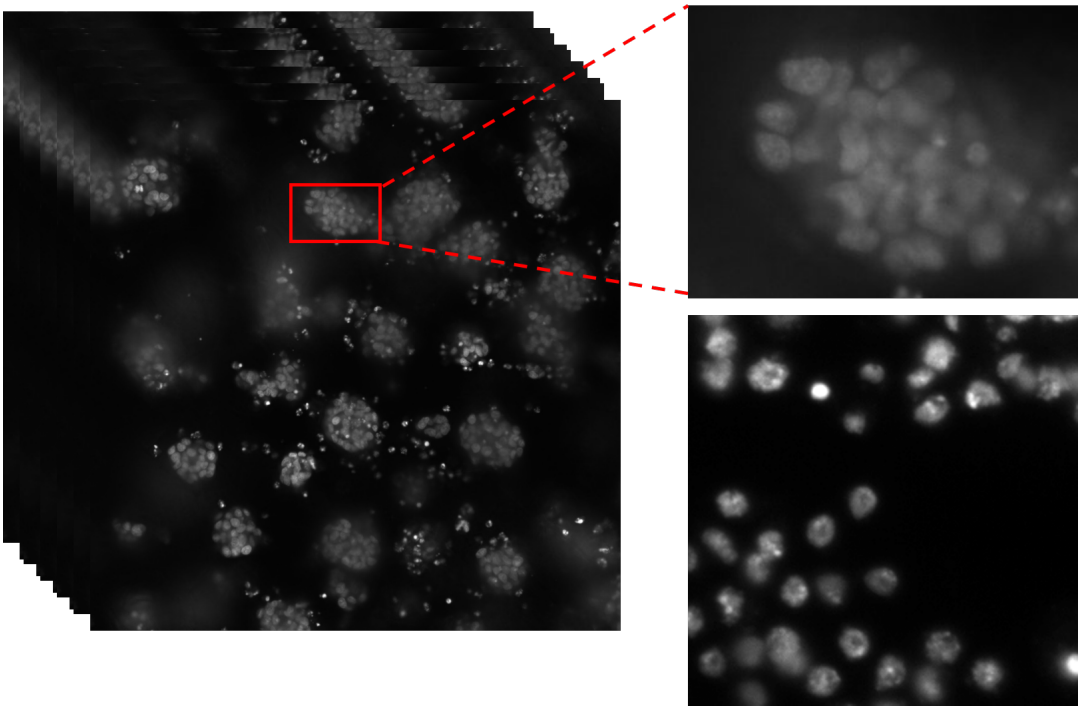

FIGURE 2.4: Microscopic images from 2D vs 3D cell culture

images of nuclei. The first one taken from a stack of microscopic images (image on the left) acquired from 3D cell culture and the second one is a microscopic image acquired from 2D cell culture. It is noticeable that it is easier to detect the nuclei inside the image acquired from 2D cell culture then the one acquired from the 3D cell culture. This is due to several artifacts inside the images as a consequence to the translucent environment where the 3D cell culture is developed. It raises the need to develop automated systems that can aid the biologists in their manual analysis.

2.4 Conclusion

Cerivcal cancer is a tumoral disease that affects women worldwide. This type of cancer may be benign if detected at an early stage and have a survival rate of 92%. However, it could be terminal if detected at a later stage and cancerous cells spread beyond the cervix area. The chance of survival drops to 18%. Different cancer treatments are available to help contain the tumor and try saving the patient, however the side effects of such treatments may be harmful. This urge the scientific community to develop new treatments that are safer and give a higher survival rate for terminally ill patients. To achieve such advancements, the dug discovery process must

be improved since it takes a significant amount of time and money to create a single drug. Working with 3D cell cultures is very beneficial to study the effect of a certain drug on the cells since this in-vitro process mimics the in-vivo environment and preserves the cells morphology and functions. However, the complexity that comes with working in a 3D cell culture affects the manual observation of the biologists. Indeed, the artifacts that are seen in the huge amount of the acquired images prevent the experts from conducting their study. There is a need to develop automatic methods based on learning processes that can help experts evaluate drugs efficiently in a 3D culture of cancer cells. Having robust methods that can detect and segment the cell components inside microscopic images can be a first crucial step followed by a 3D reconstruction since we are working in a 3D cell culture. Detecting, segmenting and reconstructing the cell components can help conduct a morphological analysis on the changes that occur during a drug testing on cancer cells. The next chapter will elaborate in details the available automatic methods that can achieve such tasks and the contributions that we made to help improve the results.

Chapter 3

Machine learning based comparative analysis of nuclei segmentation from 3D cell culture microscopic images

3.1 Introduction

One of the pathological challenges through history is Cancer, a disease defined by an abnormal growth of cells that can spread through the entire body. Cancer is the second leading cause of death worldwide that killed approximately 10 million people in 2020. With 300 000 new cases among children yearly, the estimation of the annual economic cost spent on cancer in 2010 goes up to US$ 1,16 trillion [16].The cancer drug society [18] estimated 1,9 million new diagnosed cases and 609 360 new deaths in the United States alone. Although treatments, such as Endocrine Therapy and Cytotoxic Chemotherapy, are available to eradicate or stop the spread of cellular cancer, patients can still suffer from side effects. According to a 2019 review on concepts to reduce the side effects of systemic cancer treatment, symptoms are divided into grades from 1 to 4. With grade 1 signifying mild intensity and grade 4 as life threatening. These effects can have direct health impact on the skin, hair, blood, kidneys as well as the heart, the lungs and brain. Grade 3 and 4 also suggest paralysis, spasms and coma. Some chronic chemotherapy effects are also pointed out such as drug resistance and infertility [66]. This highlights the need to develop

more effective and less toxic pharmacological treatments for cervical cancer. However, drug development is expensive. The cost for the development of a single drug can range from 161 million to 1,8 billion United States dollars [56]. According to the Food and Drug Association (FDA) of the United States, the drug development process typically involves five stages: early drug discovery, preclinical research, clinical research, pre-marketing drug FDA review, and post-market drug safety monitoring by the FDA [24]. It takes around 12 years in the United States between the start of the preclinical tests and the drug's market release, taking into consideration the FDA's drug safety approval [75]. Therefore, this is a massive amount of time and money for an uncertain release of a medication and the consumption of these resources should be reduced. It highlights the need to develop techniques to speed up the process without compromising on the safety.

One reason why the process is so difficult comes from the high failure rate at the clinical research step. Almost 2/3 of drug candidates are rejected at this step due to toxicity in humans (20%) or lack of efficiency (30%). As described in the review of A. Langhans et al. [48], the gap between preclinical research and clinical research can be explained by the non-physiological conditions of in vitro tests in preclinical research steps (early stage drug discovery). Indeed, cellular assays are usually performed with 2 dimensional monolayers of cells, which is completely different from the organization of cells in vivo, in the human body. It is now well established that three-dimensional (3D) cell cultures better mimic the structure and the behavior of human tissues [62] because they take into account (i) the interconnections between cells, (ii) the 3D structure of tissues and (iii) the extracellular matrix (ECM) surrounding the cells.

Over the past decades, 2D cell cultures were used because of their low cost and technical ease of use. More and more 3D cellular models are made available, based on different cell culture systems without physical support for cells (e.g., ultra-low attachment plate) or with support in different forms (solids scaffold and hydrogels of different origins). In this study, we focused on BIOMIMESYS® Hydroscaffold (HCS Pharma, Loos, France), a physiological 3D cell culture system based on native extracellular matrix components (hyaluronic acid, collagens, adhesion proteins or peptides). Associating the behavior of a solid scaffold and of a hydrogel, it provides

a relevant microenvironment for 3D cell culture ([9]) in which cancer cells usually grow as spheroids[12].

A powerful, cellular-based, drug discovery method lies in High Content Screening (HCS) [59]. HCS, also known as High Throughput Imaging, works at the cellular level by quantifying the characteristics of the cellular changes among a single cell or population of cells while going through chemical treatments, by using microscopy. These modifications are converted into data and used for analysis [50], allowing to conclude on the effect of any treatment on the cells in terms of toxicity and/or efficiency. These data can be extracted from pictures acquired using automated fluorescence microscopy. Fluorescence microscopy is based on a physical phenomenon called fluorescence, i.e. the emission of light just after absorption of a photon from an "excitation light". Rare biological tissues have this property. Therefore, to visualize cellular or subcellular structures, the use of fluorescent molecules (called fluorophores or fluorochromes) which are able to interact with specific biological molecules of interest is needed. In this study, we used Hoechst fluorochrome, adapted to observe cell nuclei, since it can go through the cell membrane and binds strongly to adenine–thymine-rich regions in DNA [49]. However, the large number of pictures arising from automated fluorescent microscopy is time-consuming and complex to analyze by biologists, and the interpretation can be complicated for concluding about the effect of a treatment, which requires the aid of advanced computational tools. The first required step is the segmentation of pictures. It aims at locating and contouring the needed elements. Automatic Analysis proved a big advancement in the cellular field with accurate quantification of cells features and information [2]. Cellular Segmentation is a significant step in the cellular analysis. Having a good automatic segmentation procedure, can result in a time reductive analysis system for thousands of microscopic images, thus having a better drug analysis efficiency. Machine Learning methods showed important results in segmentation with the use of different architectures but can be improved to get an accurate representation of the studied element. Focusing on computational learning methods for drug screening on cancer cell microscopy, this comparative study for nuclei segmentation will be based on different machine learning architectures through the Waikato Environment for Knowledge Analysis, followed by image manipulations

and metrics evaluations on nuclei microscopic images. These images come from a 3D cell cultures of cervical cancer cells (HeLa cell line, ATCC® CCL-2™) grown in BIOMIMESYS® Oncology. This will demonstrate and clearly show the application, competence and limits of machine learning methods on fluorescence microscopic segmentation and the need to go into more complexed architectures.

3.2 State of the Art

Several studies have evaluated the performance of different machine learning tools for the segmentation of nuclei in cervical cancer cells.

In this section, we are going to look at recent studies on cellular segmentation analysis in microscopic images. First, we will tackle some experimentations related to segmentation on cervical cancer microscopy to have an idea about the work done on this specific tumor. Then, we will cite different studies based on pixel's classification segmentation while mentioning the Fiji software and the Trainable Weka Segmentation plugin. These industrial tools are reliable to biologists who are not experts in artificial intelligence. Different articles also proposed comparative studies based on machine learning and deep learning techniques. In the end, we will introduce some applications of pure deep learning techniques for cellular segmentation that will be a road path to our future work.

Different applications, aiming for cervical cancer screening, are available. Here are two selected studies related to microscopic segmentation. The first one, is an experimentation on nucleus detection and segmentation presented with the means of a superpixel and CNN architectures [85]. After a coarse segmentation using Otsu's thresholding method, Song et al. exploited the superpixel segmentation (based on a group of pixels that shares the same characteristics). The superpixel segmentation is well known for low contrast segmentation thus helping in reducing the bad illumination and uneven staining. They also used a CNN to extract features that can represent a cervical cancer cells (superpixel, shape, color, size, etc.). The experimentation was tested on 200 women subjects. The total CNN training set was formed from 1200 cells and 200 cells for testing represented in images of 1024x1360. It leads

to an accuracy of 0,94 for the nucleus detection and a precision of 0,91 for the segmentation. Another study presented an unsupervised approach for a segmentation and classification of cervical cells [34]. The process was based on a thresholding method to differentiate between the cells and the background. Then a multi-scale hierarchical segmentation was presented to separate the region of interests in terms of homogeneity and circularity. A binary classifier was later added to separate the nuclei from the cytoplasm. They achieved an accuracy of 96,71%. They concluded that, a multi-level segmentation could improve the performance of the classifiers that work best using a KNN combined with other techniques such as SVM or a pixel level classification. Some experimentations were performed through imaging software analysis. A published paper by D. Sikpa et al. [69] shows automated methods for detecting breast cancer brain metastases in an animal model. The experimentation consists of 100 H&E stained microscopy images of brain sections showing various level of brain metastases. The microscopy was done with a 40-x magnification. The Trainable Weka Segmentation plugin in Fiji was used for the segmentation process through a pixel's classification. They added six segmentation classes: Normal Brain, Metastases, Ventricles, Artefact, Void, and Frame. For the training process, the default random forest architecture was selected. A manual segmentation was performed on the images to have a ground truth for evaluation. They discovered that a coefficient greater than 0,8 was detected with the person's correlation coefficient while comparing the segmentation result and the ground truth. Another article [8] published by D. Baltissen et al., compares different segmentation methods for glioblastoma cells. The experimentation was established on 50 fluorescence microscopy images through a confocal microscope with 63-x objective lens. Nine different segmentation methods were implemented. The best results were obtained with two different models: the first one trained on the random forest using the WEKA software, it gave a Dice Index of 0,914. And the second one, a deep learning method, with the U-Net architecture that gave a Dice Index of 0,925.

Some segmentation procedures, such as the Trainable Weka Segmentation mentioned earlier, are based on pixel classification. A research stated a new architecture for pixel classification. The study carried out by De Xie et al. [26] talks about nuclei

segmentation in microscopic images using deep machine learning. This segmentation method is a multi-pixel classification with a CNN architecture (that showed interesting results in classification problems). The experimentation was conducted on, 2000x2000, 141 images with 141 binary masks. They compared the Alex Net and the VGGNet. with their own Multi Pixel Classification architecture. Their method is based on enlarging the area that is being evaluated on a group of four pixels and sum the labels of these pixels group to have a value between 0 and 4. They used the F-score metric that gave a similarity coefficient of 0,9 for the VGG and Alex Net and a 0,8 for the Multi-pixel classification. A similar article based on active learning published by Wen et al. [79] shows a comparative study of different classification architectures for nuclei segmentation. Active learning is a semi-supervised learning where the user can provide new labels through the learning process. They worked with the SVM, Random Forest and CNN architectures through an active learning procedure. This experimentation was evaluated on whole slide image breast cancer tissues and pancreatic cancer tissue. They concluded that the CNN has shown a better performance with higher accuracy but took more time to train. They proved that more they added patches into the training system better was the accuracy. They reached more than 90% with the addition of 400 patches. It is noticeable that several researches nowadays use deep learning architectures to achieve segmentation. From the most relevant work, an article on deep learning implementation for nuclei segmentation, published by Naylor et al. [57]. They presented the results of different deep architectures like the PangNet, the ConvNet and the FCN in nuclei segmentation. Their study was based on 33 512x512 annoted HE stained histopathological images with 2754 annoted cells. They tested the three architectures on these images. They came up with a conclusion that, deeper networks such as the FCN and DeconvNet learned better then the Pang Net. The results proved that these kind of architectures worked great into recognizing nuclei but still far from dealing with the overlap issue. They used several similarity metrics for the evaluation and got an average of 0,8 similarity coefficient with the F1 score and the Jaccard Index. Another study realized by Fishman et al. [33] is about nuclei segmentation using of neural networks. They evaluated the performances of three architectures: U-Net, Mask R-CNN and Deep Cell. Their dataset was formed of 16 images with 288x288 pixels

each from a brightfield microscopy of seven different cell lines. The study showed that the U-Net architecture gave the best performance on the different cell lines with an accuracy of 89 to 97% and the F1 score, evaluation metric, of 0,76 to 0,86. The mentioned works offered different examples of learning methods and architectures that proved an advancement in automatic segmentation techniques. The work presented in this study will be a comparative study between three machine learning architectures, the Random Forest based on predictive trees, the Adaboost based on Boosting method and the MLP based on Artificial Neural Network. This study will evaluate and compare the performances of these different kind of methods through the aid of Fiji and WEKA tools suggested by the company HCS Pharma.

3.3 Dataset, Methods and tools

Through this comparative study, different softwares have been used for this experimentation. Fiji, an image analysis software and WEKA a learning tool aided in the data collection and learning process. Different machine learning architectures were exploited in this work to achieve an auto-segmentation. The Random Forest, Adaboost and MLP were used to have a comparative segmentation analysis. This comparison was evaluated later by two evaluation metrics: The Dice Coefficient and the Jaccard Index[74]. These techniques compare two images and give a coefficient between 0 and 1 to evaluate the similarity between them. For these experi mentations, an Intel(R) Core (TM) i7-6700HQ CPU @ 2.60GHz was employed.

3.3.1 Dataset

The initial dataset is composed of nine microscopy images with 20-x magnification divided into six images as a training set and the remaining three images as a testing set. Three biological Experts from HCS Pharma manually segmented these images based on their expertise to form a set of groundtruth. The six training images and the ground truth for each were used to create our training data. We created a data file For each training image and one of its corresponding ground truth. Each data file is composed of pixels information and the corresponding class for each pixel (Class 1: Nuclei, class2: other).

3.3.2 Evaluation Metrics

The Dice coefficient and Jaccard indices were used to assess the quality of the segmentation in relation to the ground truth. The Dice Coefficient, also known as the mean overlap (MO), was calculated using the following formula [74]:

$$MO = 2\frac{\sum_r |S_r \bigcap T_r|}{\sum_r |S_r| + |T_r|} \tag{3.1}$$

The Jaccard index, also known as the union overlap (UO), was calculated as follows:

$$UO = 2\frac{\sum_r |S_r \bigcap T_r|}{\sum_r |S_r \bigcup T_r|} \tag{3.2}$$

For both equations, S represents the segmentation set, T is the ground truth set, and r represents the entire region. A value of 1 indicates a perfect overlap, while 0 indicates no overlap.

3.3.3 Software

Fiji– Fiji is an open-source image analysis software based on imageJ [14]. A set of plugins are available through this platform to achieve different tasks for image manipulations. One of these plugins is the Trainable Weka Segmentation (TWS). This plugin is often used to train and test machine learning algorithms and to perform image segmentation with pixel classification methods [5]. This plugin, developed by Waikato allows a manual segmentation, the creation of data files from images by saving pixel's information with a labeling, the application of features for data augmentation and manipulation, the training process through different WEKA based architectures and the application of models on testing images. In this work, the Trainable Weka Segmentation plugin was exploited to create data files, apply features and for the testing process later on. For the training The Waikato tool, WEKA was used.

WEKA– Waikato Environment for Knowledge Analysis known as WEKA is a machine learning tool specialized in data visualization and training [38]. Several built-in machine learning algorithms are available for the training process. For this work,

three architectures were used from the proposed list, The Random Forest, the Adaboost and the Multi-layer Perceptron. The WEKA tool was more favorable for the training process. It provides as outcome the training model with all the needed information about the training accuracy, the confusion matrix, time needed to train, etc.

3.3.4 Segmentation Methods

Random Forest– The Random Forest (RF) is a machine learning architecture based on a combination of predictive trees and considered as an efficient classification technique that works over a large dataset [11][61]. Random Forest are considered more robust in terms of noise reduction. It is stated in the article [11] that according to the law of large numbers, meaning the numbers of training iterations, it is unlikely for a random forest to overfit. Random forest gives a competitive result with boosting and adaptive bagging methods while conserving the training set through all the training progress.

AdaBoost– Adaboost is a machine learning architecture based on a boosting approach that allows achieving a higher accuracy rate by combining inaccurate and weak rules. The adaboost remains the most effective boosting algorithm that is still used and studied nowadays [65]. Adaboost algorithm, developed by Freund and Schapire in 1994, is based on classification techniques and operates by selecting the best features [70]. In this work, the default adaboostM1 in the WEKA application was used to train the dataset and create models to apply for segmentation.

MLP– The Multi-Layer Perceptron or MLP is an example of artificial neural network (ANN). ANN attempts to develop an artificial model of the human brain. An MLP is defined by a simple perceptron composed of input neurons and output neurons with an addition of multiple weight layers known as hidden layers. The distinctive point in an MLP is the backward propagation that, after calculating the error by subtracting the actual output from the desired output, it projects the obtained value backwards thus modifying the weights and improving the training performance [60]. In this experimentation, these three algorithms were exploited through

the WEKA training tool to study their performances for a pixel classification problem thus resulting in the creation of different segmentation models.

Majority Voting– In this research, majority voting was executed on the segmentation results obtained from three models (RF, AdaBoost and MLP). To this end, a global segmentation is generated based on the dominant label for each pixel, predicted by the three considered methods.

StarDist– StarDist [67] is a segmentation method for microscopic images based on artificial neural networks. This method is available as a plugin on the Fiji software. The method aims to detect cells based on their star-convex shapes. The model used in this study was trained on a subset of the DSB 2018 nuclei segmentation challenge dataset [15].

3.3.5 Features

While creating the data files through the Trainable Weka Segmentation plugin, several features were selected. These features served as data augmentation for the training set thus creating different values for one pixel in the data file. These features or manipulations are built-in the Trainable Weka Segmentation plugin in Fiji where the user can select several ones from a list. These features are divided in categories [5]:

Edge Detectors– From the edge detectors filters we can cite the Laplacian and Sobel filters, difference of Gaussians, Hessian matrix eigenvalues and Gabor filters. These filters aim into detecting boundaries.

Texture Filters– These filters aim into extracting texture characteristics. The minimum, maximum, median, variance and entropy are built-in available filters in the plugin.

Noise Reduction Filters– We can cite Gaussian blur, bilateral filter, anisotropic diffusion, Kuwahara and Lipschitz as noise reduction filters. These helps in localizing the membrane.

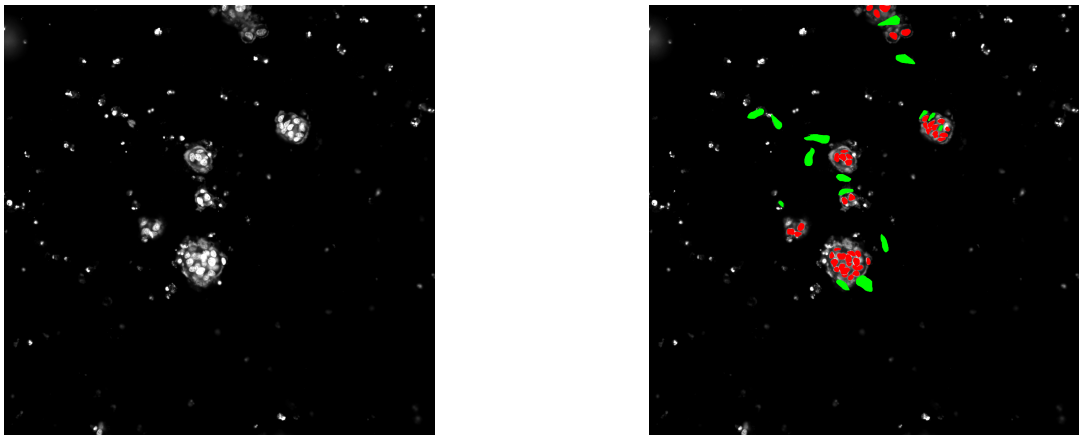

(A) Original Image (B) Manual labellisation

FIGURE 3.1: A manual labellisation performed for data collection that will be used for the training process. The regions labeled in red represents the class 1 (nuclei) and the regions labeled in green represent the class 2 (background, debris, etc.)

3.4 Experimentations

The experimentation consists of nine microscopy images with 20-x magnification divided into six images as a training set and the remaining three images as a testing set. Three biological Experts from HCS Pharma manually segmented these images based on their expertise to form a set of groundtruth. The tool, Fiji helped in the process of data collection and classes division and balance (Figure 3.1). This was achieved through the Trainable Weka Segmentation that assisted in the data division into two classes, through a manual segmentation, with the first class representing the nuclei segmented by the expert and the second class representing regions from the remains (background, noise, debris, etc.). As the second class has a larger representation in the image, a program based on the Macro language insured the data balance between the two classes. The experimentation can be summarized through these steps and is visualized through a diagram in Figure 3.2.

3.4.1 Cellular Culture and Microscopy

HeLa cells were first cultured with DMEM (Eurobio, France) supplemented with 10% (v/v) of fetal calf serum (Corning, France), 1% of non-essential amino acids 100X, 2mM L-glutamine, and 100μg/mL of penicillin or streptomycin. The cultures were seeded at 25000 cells per well in the BIOMIMESYS oncology medium

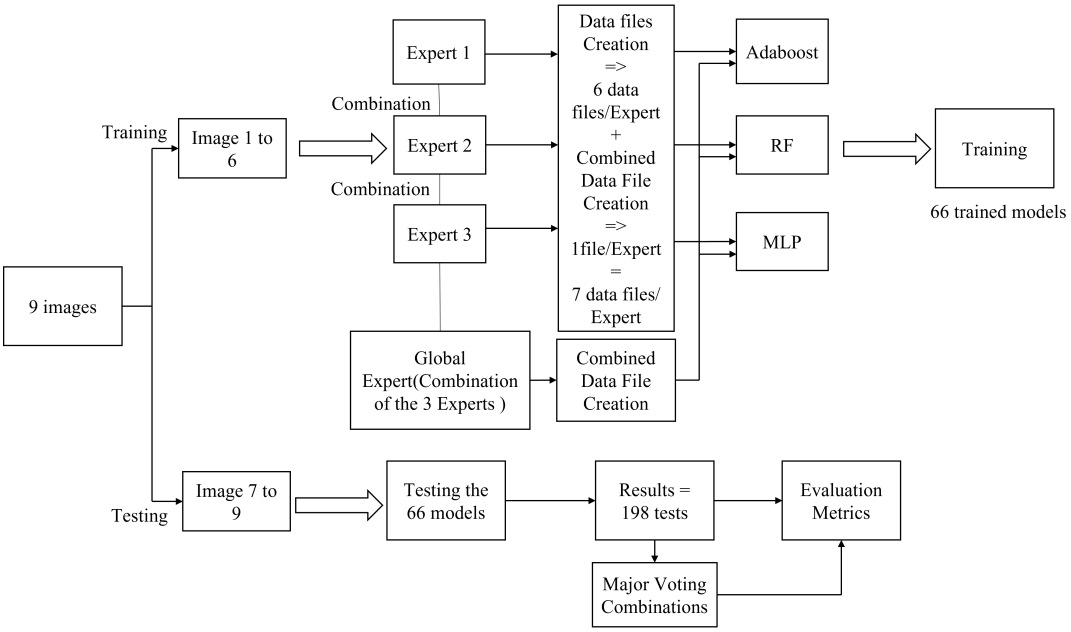

FIGURE 3.2: Diagram that represents all the experimentation process

(HCS Pharma, France). The medium was changed every two or three days. After seven days, the cells were stained with 10μg/mL of Hoechst 33342 (Fisher Scientific, France) and 2μM calcein-AM (Sigma-Aldrich, France) for 45 minutes at 37°C, in 5% carbon dioxide (CO2). The microscopy images were acquired using an automated ImageXpress Micro Confocal microscope (Molecular Devices) in confocal mode, with a 20-x "plan apo lambda" objective (Figure 3.3). In this study, we only used images made from DAPI fluorochrome. The path of the light to illuminate the samples was produced with a 377nm excitation light filter (with a width of about 50nm) and a 477nm emission light filter (with a width of about 60nm). A 409nm dichroic mirror was used to separate the beams. The spinning disk configuration was a "60μm pinhole" for the confocal mode. Each image had a 2048x2048 pixel format with an x/y resolution of 0,4μm and an axial resolution of about 6,3μm. For each site, we considered 75 pictures from z=0 (which is the bottom of the well) to z=75μm, with a 1μm increment. Most of the training of the models was performed at z=20μm as the images in this position had the best contrast resolution and therefore exhibited more objects compared to images in the other positions. However, we then tested the models on other z planes to quantify their robustness.

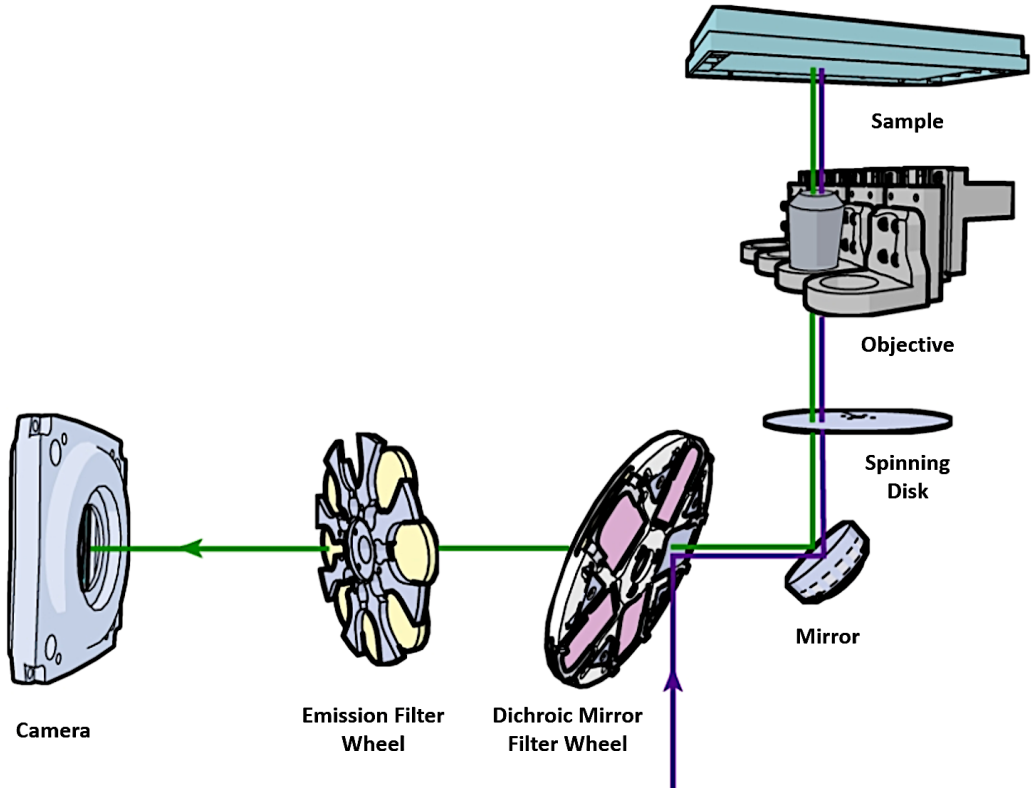

FIGURE 3.3: The principle of the operation for an ImageXpress Micro XLS microscope

	Combined Files		
Algorithm/Expert	**Expert 1**	**Expert 2**	**Expert 3**
Number of instances in each file (Training Data)	355 097	385 864	508 205
Random Forest Accuracy	99,635	99,6755	99,7954
AdaBoost accuracy	92,3663	92,6111	93,0849
MLP accuracy	91,4114	93,2598	94,3613

TABLE 3.1: The number of instances and accuracy of the models trained on the combined files for each expert.

3.4.2 Feature Extraction

Using the TWS, and based on the 6 training images, six files in the form of ".arff" (attribute-relation files format) were created for each manual segmentation done by the three experts. Then, a combination process joined the six files into one, thus creating a seventh data file per expert. All the files contained the pixel values from the manually segmented regions with the matching label and the selected training features. In total, 21 files were formed, with an average of 300000 instances and 400MB per file. The number of instances in each combined file is indicated in Table 3.1. While creating the data files through the TWS plugin, several features were selected. These features served as pixel's transformation for the training dataset, thus creating different values for one pixel in the data file. These features or manipulations are built within the Fiji TWS plugins and can be easily selected from a list and divided into three categories, edge detectors, texture filters, and noise reduction. Edge detectors are designed to detect boundaries and include Laplacian and Sobel filters and the difference of Gaussians, Hessian matrix eigenvalues, and Gabor filters. Texture filters are used to extract texture characteristics. The minimum, maximum, median, variance, and entropy are built-in texture filters that can be extracted through the TWS plugin. Noise reduction filters, including Gaussian blur, bilateral filter, anisotropic diffusion, Kuwahara, and Lipschitz help to localize the nucleic membrane.

3.4.3 Training data

Through the WEKA environment, the data obtained earlier were exploited for models' training. Each data file was trained by means of three classifiers. The classifiers were trained to learn based on the K-folds cross validation: a method used to divide the data into training and validation sets. K cross-validation folds mean that the data is divided into K groups of training and validation, and each group is trained individually. The RF (Random Forest) and Adaboost were trained using a 10 cross-validation folds and the MLP was trained using 3. These values were considered based on the default parameters in WEKA. The number of instances in each file and the performance of each model are shown in Table 3.1.

Combined Files	
Algorithm/Expert	**Global Expert**
Number of instances	393 728
Random Forest accuracy	99,653
Random forest training time	1348,7 seconds
AdaBoost accuracy	92,131
AdaBoost training time	542,74 seconds
MLP accuracy	92,575
MLP training time	1897,4 seconds

TABLE 3.2: Performances of the 3 classifiers on the global expert combined data file.

3.4.4 Testing data

The models were tested on the image located at z = 20 from the 3 stacks allocated for the test phase, thus creating a probability map for each. The binarization process was then applied to the probability maps. This simplified the manipulation and interpretation of the images later on. It was visually clear that the combined training data RF classifier provided a better segmentation result for the three experts.

3.4.5 Image Processing

Image Binarization– Image binarization is used to transform a colored image into a black and white image. More specifically, each pixel is assigned a value of 0 or 255 based on a threshold value of 127.

Global Ground Truth– The combination of the ground truth images developed by the three experts was used to create global ground truth for each of the nine original images. The same data acquisition process was then applied using these new images to create a new combined data file containing 393728 sets to train on. Then, the same data training process was performed on this newly created combined data file (Sections Feature extraction, Training data) (Table 3.2). Eventually, three new models were created through the learning of the defined architectures. Then, the same process of testing was applied using these new models. Figure 3.4 shows the original image, the global ground truth, and the probability maps for each classifier.

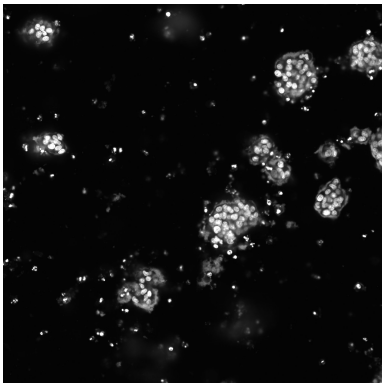

(A) Original Image

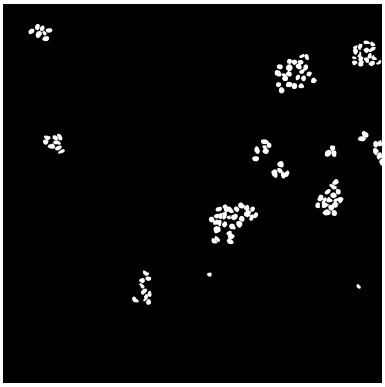

(B) Ground-Truth

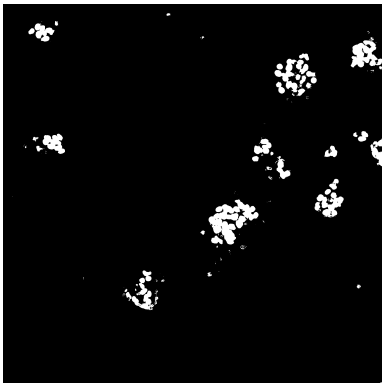

(C) RF Segmentation

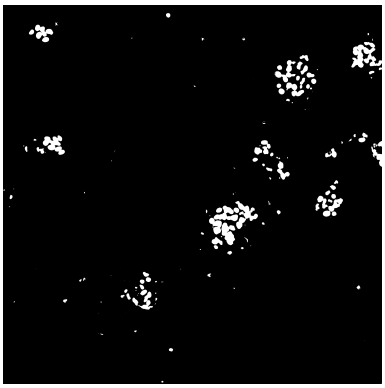

(D) Adaboost Segmentation

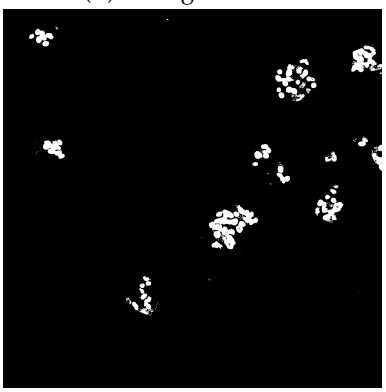

(E) MLP Segmentation

FIGURE 3.4: Segmentation results with three different classifiers

3.4.6 Multiple Z-Stack Testing

Each acquired image from the HCS Pharma is a stack of 2D images that can be reconstructed as a 3D image. Each stack is composed of 75 images. Each picture was acquired at a difference of 1μm above the bottom of the well from the plate containing 96 wells. The training and testing phases were done on the twentieth slice (at 20μm above the bottom of the well). The image at this position is not blurry, and numerous nuclei are present, hence facilitating the training of the algorithm. The models created by the learning performed on the combined files formed with the global ground truth were also tested on the 5th, 30th, and 60th slice positions. The 30th slice closely resembled the 20th slice, while the 5th and the 60th slices were blurrier and had fewer nuclei. The segmentations were visually analyzed to evaluate the performances at different levels

3.4.7 External Validation

The described process was tested on two different datasets of four images, each obtained from the HCS Pharma. The first one (referred to as Dataset A) was taken from another well of the same cellular culture plate. This dataset had the same biological and microscopic conditions as the original dataset. The second one (referred to as Dataset B) was taken from the same well as the original with the same biological conditions but with a microscopic magnification of 10-x, and hence, a different depth level. For this analysis, the second slice with dimensions of 1024x1024 was taken. The models trained with the combined data file on the global ground truth with majority voting of the models' results were used to segment the cases.

3.5 Results

3.5.1 Training Performance Accuracy

The training process showed an excellent learning accuracy higher than 90% for the three models. The RF-based classifier exhibited the best performance with an average accuracy higher than 99%, followed by the MLP with 93% and AdaBoost with 92,68%. However, the AdaBoost algorithm had the shortest training time with

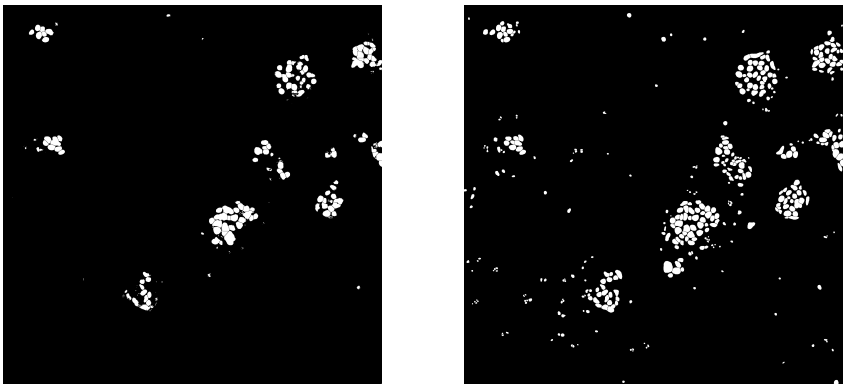

(A) Majority Voting result (B) StarDist test result

FIGURE 3.5: Segmentations results with two different methods

an average of 613,5 seconds/fold, followed by the RF with an average of 1308 seconds/fold and the MLP with an average of 1611.6 seconds/ fold. The training performed on the combined file created with the global ground truth exhibited similar accuracies for the three models, i.e., 99%, 92,5%, and 92% for the RF, MLP, and AdaBoost algorithms, respectively. However, the test experiments were more interesting in terms of results.

3.5.2 Performance of the Three Algorithms in Relation to the Global Ground Truth

The similarity rates obtained from five different methods (RF, AdaBoost, MLP, Majority Voting and StarDist) are summarized in Table 3.3. The models used to achieve these similarity rates are the ones trained on the global ground truth. MLP exhibited the highest Dice coefficient (0,805), followed by AdaBoost (0,782) and RF (0,771). Similarly, MLP had the highest Jaccard index (0,675), followed by AdaBoost (0,642) and RF (0,627). After applying the majority voting technique, the combined models trained on the global ground truth achieved the highest performance with a Dice coefficient of 0,807 and a Jaccard index of 0,676. The evaluation metrics applied on the StarDist resulting image and the global ground truth provided a Dice coefficient of 0,615 and a Jaccard Index of 0,444 (Figure 3.5). A true positive, false positive, and false negative rates representation is illustrated for each segmentation result in Figure 3.6.

Methods	**RF**	**Adaboost**	**MLP**	**Majority Voting**	**StarDist**
Dice Coefficient	0,771	0,782	0,805	0,807	0,615
Jaccard Index	0,627	0,642	0,675	0,676	0,444

TABLE 3.3: Segmentation performance in terms of similarity metrics obtained by the five ML methods.

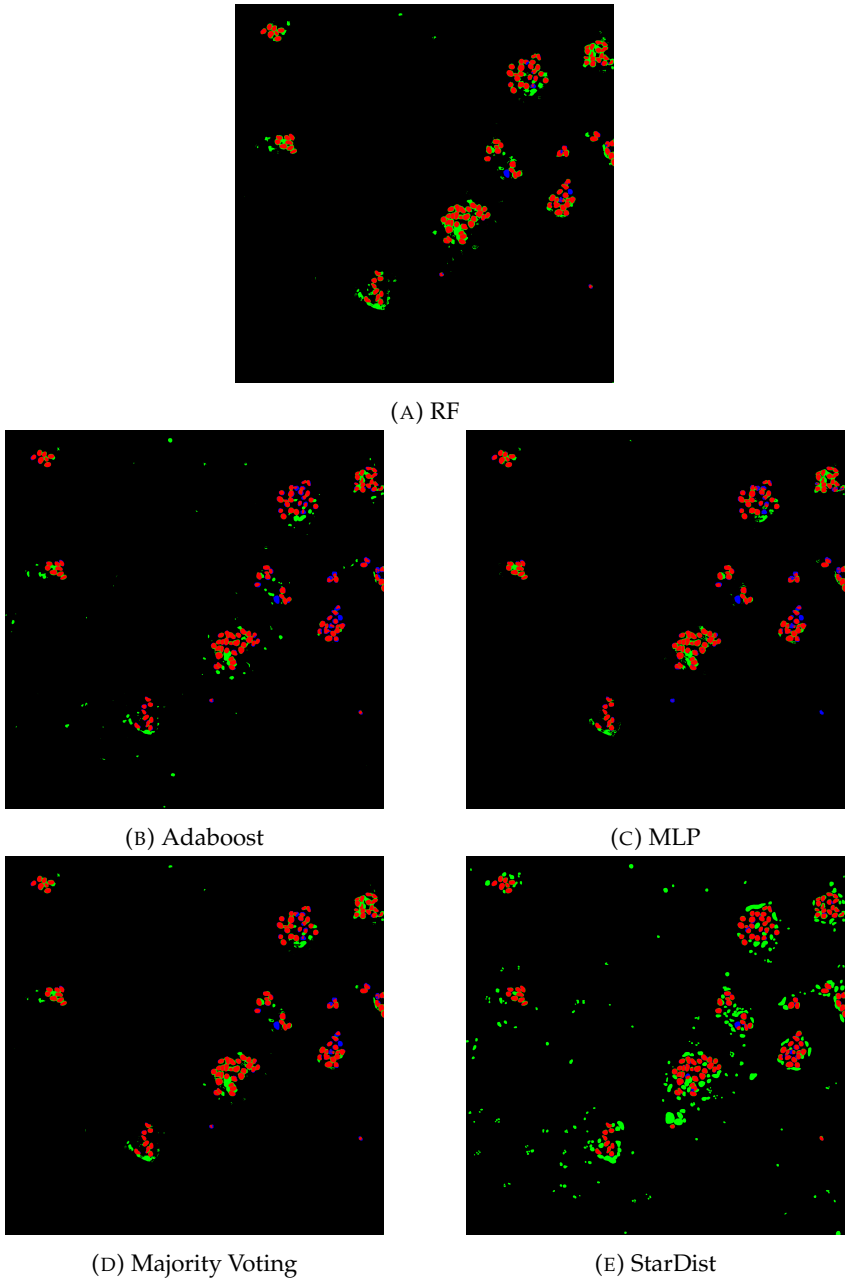

(A) RF

(B) Adaboost

(C) MLP

(D) Majority Voting

(E) StarDist

FIGURE 3.6: Visual representation of the positive and negative rates on the segmentation results. The TP (True Positive), FP (False Positive) and FN (False Negative) are labeled in red, green and blue, respectively.

3.5.3 Z-stack Evaluation

For the Z-stack evaluation, the auto-segmentation based on the majority voting of the three classifiers was applied as it provided the best performance. A visual analysis of the Z-stack evaluation in Figure 3.7 shows a good segmentation on the 30^{th} slice and an inaccurate segmentation on the 5^{th} and the 60^{th} slices.

3.5.4 Multi-Datasets Testing

The results regarding the multi-datasets majority voting in relation to the ground truth provided by an HCS Pharma expert are illustrated in Figure 3.8. The image segmentation on dataset A provided a Dice coefficient of 0,7059 and a Jaccard index of 0,5455, while the image segmentation on dataset B provided a Dice coefficient of 0,4781 and a Jaccard index of 0,3141.

3.5.5 Morphological Analysis

Morphological analysis was performed using the particle analyzer plugin in Fiji. We set the parameter that took into consideration the number of pixels needed to form a certain nucleus. This parameter was empirically set to 100 pixels to detect all the possible nuclei.

3.6 Discussion and challenges

As shown in Table 3.1, the random forest classifier achieved the best accuracy performance with a precision higher than 99%. However, in the testing phase the MLP gave the best similarity evaluation with the global ground truth process with a Dice Coefficient of 0,8062 and a Jaccard Index of 0,6753. Through a visual analysis in Figure 4, it is clear that the models succeeded in removing almost all noise and debris from the image but still need improvement for detecting and separating overlapped area. With the Majority voting technique for the ground-truth and the three segmentation outputs, the best result gave a slightly better similarity value than the MLP with a Dice Coefficient of 0,8065 and a Jaccard Index of 0,6758. Visually in Figure 3.5a , some nuclei can be distinguished on the image; this indicates the decrease

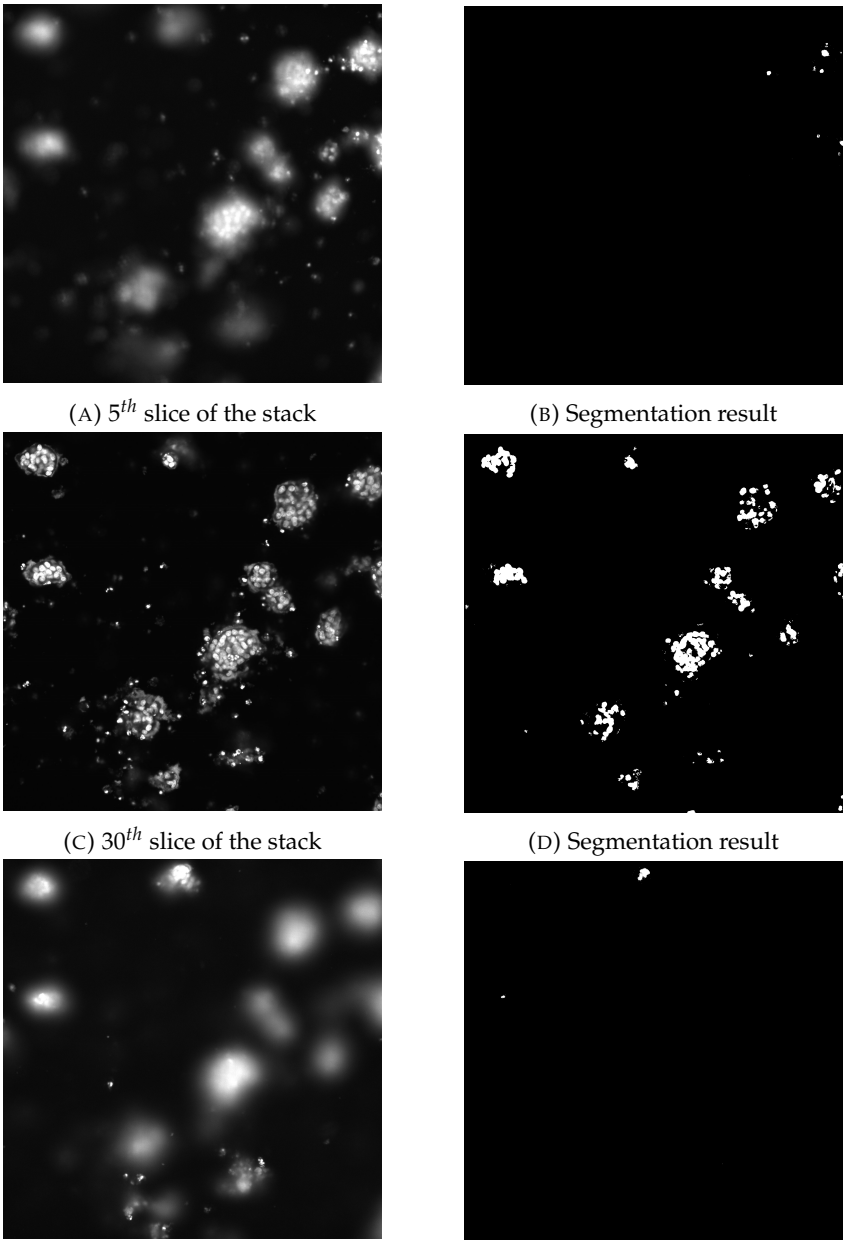

(A) 5^{th} slice of the stack (B) Segmentation result

(C) 30^{th} slice of the stack (D) Segmentation result

(E) 60^{th} slice of the stack (F) Segmentation result

FIGURE 3.7: images from the same z-stack at different positions with their corresponding majority voting segmentation results.

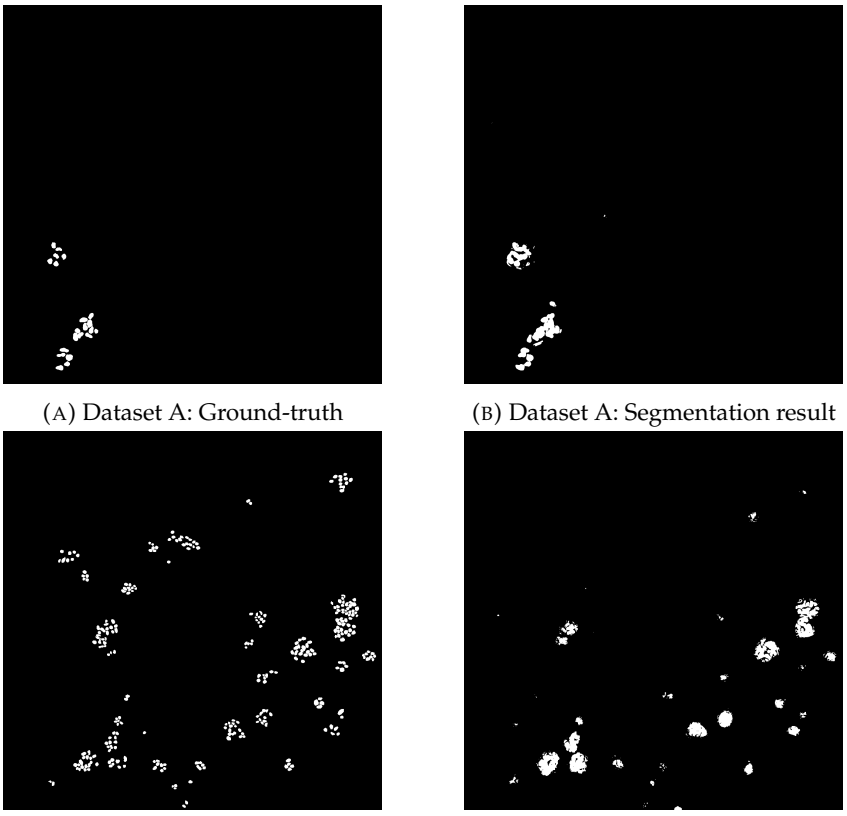

(A) Dataset A: Ground-truth

(B) Dataset A: Segmentation result

(C) Dataset B: Ground-truth

(D) Dataset B: Segmentation result

FIGURE 3.8: Majority voting segmentation results with the corresponding ground truth of two images taken from two different datasets: Dataset A that provides the same condition as the original dataset and Dataset B that represents the same set as the original dataset with microscopic magnification of 10x

of overlapping. Using StarDirst plugin, a different auto-segmentation resulted in a Dice Coefficient of 0,6149 and a Jaccard Index of 0,4439 but it is clear visually in Figure 3.5b, that this segmentation method succeeded in handling the overlap issue but did not remove the noise and debris that are present in the image. It is important to understand and to measure the difference between positive and negative rates in our segmentation results. False Negative means that the nucleus is labelled by experts but not recognized by algorithm. It is very problematic because, the nucleus truly exists. False Positive means that the algorithm finds a nucleus, but experts didn't see it. As expert's annotation is subjective, this type of error is less important in our case. Figure 3.6 represents these rates on the obtained segmentation results. On the Z-Stack testing, the visual interpretation clearly favored the segmentation performed on the 30^{th} slice while the segmentation performance was poorly represented on the other two slices. This is due to the big resemblance of the 30^{th} and 20^{th} slices in terms of nuclei and blurriness representation. It is difficult to estimate the sensibility of this method to the blurriness of object. This blurriness is linked to the depth of field of used objective which is around 5μm in confocal mode (given by the manufacturer) and to the optical absorption and diffusion capacity of the translucent medium (unknow). Visually the similarity between the 20^{th} and 30^{th} slices indicates that the second cause of blurriness is much less important than the first. Thus, it is logical that the segmentation on the 30^{th} slice gave a better result than on the 5^{th} and 60^{th} slices. To obtain a better interpretation of the process, the system was applied on different other datasets. The results obtained on the Dataset A were better than the ones obtained on the Dataset B. This is due to the fact of the huge presence of nuclei in the images in Dataset B, which was difficult to the trained models to predict. With a dice coefficient of 0,7059 and a Jaccard Index of 0,5455, the auto-segmentation performed on the Dataset A was better, since it presents the same conditions as the trained-on images. Although, this experimentation provided relevant and robust results in auto-segmentation, some improvements can be applied to attain a better performance thus achieving a better segmentation result. In Table 3.4, the conversion results from pixels to "nucleus" are presented for several images using the methods described above. We considered the number of pixels from the Global Ground Truth as the "reference" as it combines all nuclei labeled by

Image	Number of Nuclei found
Global Ground Truth	131
Majority Voting	120
MLP-Global Expert	115
STARDIST	226

TABLE 3.4: The morphological study table representing the number of nuclei in each of the following segmentation output.

experts. The global expert majority voting based on the three classifiers and "MLP-Global Expert" achieved results similar to the reference gold standard but failed to identify some of the nuclei, leading to a high false-negative rate. On the other hand, the StarDist (with or without watershed) identified more nuclei than the reference gold standard as this method tends to overestimate the number of small and bright objects (debris), leading to a higher false-positive rate. However, it is important to note that the labeling of nuclei by experts can be subjective. This could potentially influence the accuracy of the ground truth and potentially limit the results of our research findings.

3.7 Conclusion

In this experimentation, a comparison between three different machine-learning architectures was proposed, to evaluate the segmentation performance on microscopic images. The study confirmed the advancement and the relevance of the presented architectures that became more valiant with the application of a post processing technique that combines different images. These architectures proved a decent result in terms of noise reduction and classes' classification (low ratio of false negative objects without a critical augmentation of false positive) but still needs improvement to handle the overlapping issue between the nuclei. The result obtained with StarDist shows that this deep learning plugin succeeded in the overlapping issue but failed to remove all debris and non-nuclei organisms (very high rate of false positive). A different problem was also presented in this study, which is the Z-Stack segmentation. Results proved that similar or close slices could achieve the same performance in terms of segmentation. However, as it goes up or down into the different 2D

layers, the performance starts to lower in terms of segmentation. The same interpretation goes to the multi-dataset testing, with a decent segmentation performance on similar datasets that have the same conditions. However, this performance reduces in efficiency with different conditions as microscopic condition in this case. In a HCS 3D screening with thousands of 3D images, this limitation implies to increase the number of labelled images by experts (at several Z height and for several close conditions of acquisition). The time for annotation also increases and, as we have to train models on much more instances, the training time dramatically grows. It suggests that this method fits very well with homogeneous 3D screening with a small depth of work compared to the blurriness capacity of the medium. In a future work, an investigation will be conducted on these problems. First, regarding the improvement of nuclei separation, some combination processes can group the two results obtained thus maybe creating a better segmentation that can solve both issues. On a second hand, a deep learning architecture can be a path to overcome the Z-stack problem and the multi-dataset problem by creating a robust architecture that takes into consideration the different layers properties.

Chapter 4

A deep learning-based framework for the 3D reconstruction of nuclei

4.1 Introduction

As discussed in the previous chapters, cell culture is a fundamental process in drug discovery that allows the experimentation of new drugs and the analysis of the effect of chemical substances on the cellular structure. 2D cell culture is widely known and used in scientific breakthroughs due to its simplicity and low-cost [44]. However, this technique does not fully represent the physiological characteristics of the cells leading to a limited biological interpretation of the effectiveness of a candidate drug [37]. This sparked the urge to introduce 3D cell cultures [13]. Indeed, this technique has shown its ability to ensure cell to cell communication and interaction which permit to better mimic the tissue structure as well as function [37]. With the biological progress in 3D cell culture, computer vision for 3D microscopy analysis became an essential task to meet the needs of biologists. Neverthless, the translucent environment of this type of culture results in the acquisition of microscopic images with a heavy blurriness amount leading to a high complexity level. The acquired microscopic images are affected by several artefacts impacting the visual appearance of the cell environment objects. Figure 4.1 illustrates the degraded visual quality of such type of images (bright-field images) while emphasizing blurred objects namely spheroids (see on the left the first slice of the z-stack images). The figure shows also the complexity of distinguishing the nuclei due to their confusing contours (see on the right, the nuclei of one spheroid). In addition, the 3D information generated by

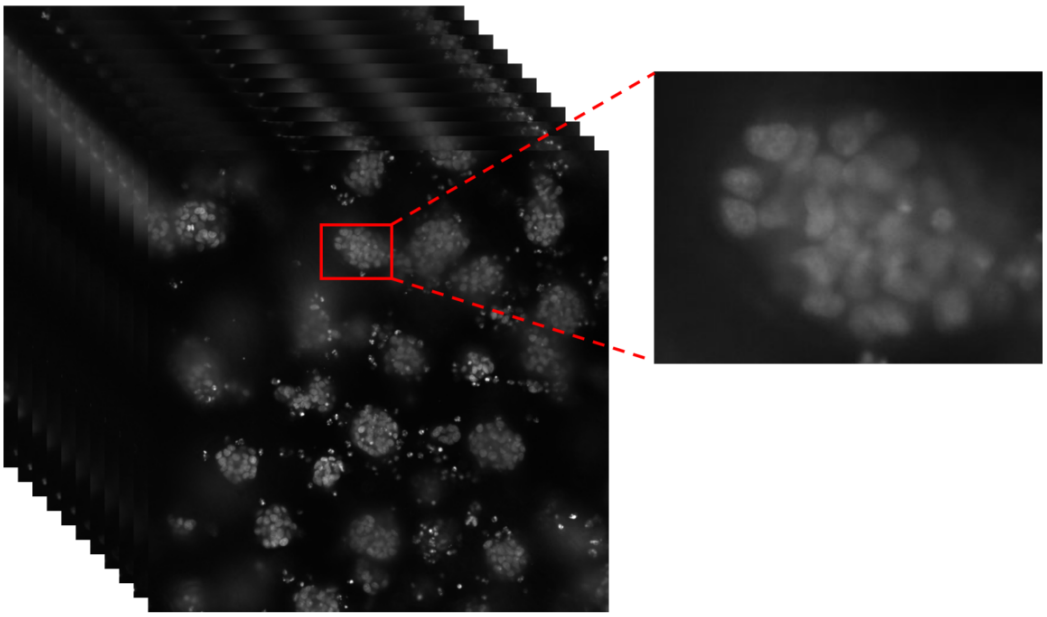

FIGURE 4.1: A z-stack images of 3D culture HeLa cells showing blurred spheroids on the left and a focus on the nuclei of one spheroid with confusing contours on the right.

the depth propagation along the z-axis of the confocal microscopy remains insufficient to guarantee a faithful representation of the whole environment notably with regards to occluded objects (spheroids hidden by other spheroids located at the same 2D position with different zdepth). All these observations make the automatic analysis of these images a great challenge and leads to the inability of visually detecting the nuclei inside these images, thus making it difficult to do a manual segmentation. Here comes the need to develop an approach to help overcome these challenges.

As discussed before, there is a need to develop automatic segmentation tools as nuclei segmentation is a fundemental step for the 3D reconstruction [41]. Deep learning architectures such as U-Net could be exploited to address the segmentation task [15] [52]. Indeed, These algorithms are well known in the field of medical imaging segmentation and have demonstrated a high efficiency [63]. However, this type of approach is well adapted for analyzing: 1) data caracterized by a single level of semantic information (for instance a population of cells or a population of nuclei) which is not the case of our 3D culture-based images. More precisely, the images contain two levels of semantic information, namely a population of spheroids, each of which representing a population of nuclei. 2) a population of separated objects with regular shapes which is also not the case of our 3D culture-based images as

highlighted in Figure 4.1. This also raises the problem of preparing a training dataset with manual segmentations of all the nuclei.

To overcome these limits, we introduce a hierarchical deep learning framework for the nuclei 3D reconstruction from a stack of microscopic images. The framework goes through three successive stages namely: at the slice level of the stack i) the spheroid detection and ii) their nuclei segmentation then at the stack level iii) nuclei 3D reconstruction. In fact, our observation on the multi-level semantic information that characterize our data has motivated our strategy of hierarchical analysis where spheroids are first detected and then their nuclei are segmented from each slice in the stack. We precise that we chose to detect spheroids instead of segmenting them because they represent an agregation of small objects (nuclei) without a continuous contour. To deal with the confusing contours of the nuclei, we propose to segment only the most visible nuclei having explicit contours. Indeed, we make the assumption that the fact to detect all the spheroids, to partially segment their nuclei from each slice in the stack and then apply a 3D reconstruction on the segmented nuclei should permit a relevant quantitative data analysis. More specifically, having an assisting tool for quantifying the number of spheroids and measuring their sizes offers to the biologists a first level of interpreting the effectiveness of a drug. Furthermore, the identification of some nuclei inside each spheroid will offer a second level of analysis with respect to their morphology. To demonstrate the efficiency of our framework, we prepared a dataset of bright-field microscopic images acquired from in-vitro 3D culture of HeLa cells (cervical cancer cells cultured in our laboratory). The images have been manually labeled by experts for both tasks namely spheroids detection and nuclei segmentation. It is worth mentioning that the partial manual segmentation of nuclei still allowed to train a segmentation model on a weakly-labeled dataset. The conducted experiments on our dataset shows the promising results of our framework notably outperforming direct nuclei segmentation methods. Our dataset and source code will be made available upon request.

4.2 State of the Art

Over the years, various studies aimed to reach spectacular performances in 2D and 3D nuclei segmentation with the means of handcrafted or deep learning methods [41]. Nevethless, working with 2D nuclear microscopy images is widely common due to the simplicity and availability of the data. So as as raised in [41], countless approaches were proposed to answer to this problematic. In this context, the paper of J. C. Caicedo et al. is based on a 2018 competition known as the 2018 Data Science Bowl contest [15]. The objective was to build a segmentation method that can be applied to any 2D light microscopy image of stained nuclei. It revealed the high interest shown by the scientific community on this task. Indeed, as indicated in [15], the contest has attracted 3,891 teams worldwide challenged on a dataset of 841 2D images containing 37,333 nuclei manually annotated. The evaluation protocol established in the frame of this contest has shown that the best performing solution was based on a variant of the U-Net deep learning architecture developped by A. Buslaev et al. This latter result has motivated the community to pursue the efforts on the development of new variants of U-Net architecture such as Cellpose [72] and StarDist [67]. For example, cellpose is a generalized algorithm for cell segmentation where the training dataset consisted of fluorescent-labelled proteins images, bright-field cells microscopy images, images of membrane labeled cells, images from other types of microscopy and non-microscopic images such as fruit, rocks and jellyfish. The training architecture was based on the U-net model. However, these methods are not adapted to perform an efficient nuclei segmentation from 3D culture-based images in reason of their strong hypothesis with regard to the analyzed patterns. More specifically, they are designed and trained to segment a population of patterns sharing all the same shape (a repetetive shape) and having explicit contours.

With that being said, some studies were adapted to 3D stack images acquired from 3D cell culture. Błażej et al. [64] have proposed a 3D reconstruction method of the nuclei surface from a z-stack images. To this end, they adopted a 2D image analysis approach that aims to delimit the contours of the nuclei from one image slice and to track their continuity over the stack to reconstruct the final surface. For the contour delimitation (nuclei segmentation) they exploited hand crafted geometric

features that permit to generate a set of boundary points. As raised by the authors, the proposed method performs well for nuclei with convex shapes and with the assumption that for each reconstructed 3D nucleus object there exist at least one 2D slice where the considered object is well separated. Wu et al. [82] proposed a deep learning method to detect and quantify the 3D nuclei centers from 3D fluorescence microscopic images. They based their calculations on the estimation of 2D centroids of these objects from 2D slices. The authors raised that the performance of their detection method is affected by irregular forms such as nuclei with non ellipsoidal shapes or when it is exploited in an image with a high-density distribution of nuclei. Maylaa et al. [55], proposed a comparative study of several hand crafted machine learning methods for the segmentation of nuclei from a z-stack image acquired from 3D cell culture of cervical cancer cells. For this purpose, they trained several classifiers that allow to identify nuclei objects pixels from one slice image and reconstruct final objects. As raised by the authors, although the trained classifiers succeeded to detect the nuclei pixels they failed to delimit the nuclei contours resulting in a blob-like objects. The obtained results in the afformentioned works on 3D culture cells show that nuclei segmentation and reconstruction tasks are still challenging and require the development of new efficient methods. This observation has been also confirmed in the recent survey [41]. Moreover, the survey highlighted also the lack of public datasets as well as manual annotations.

Regarding spheroids detection from 3D cell culture images, recently Grexa et al. [36] proposed rather to segment the spheroids by exploiting several techniques namely classical ones (Otsu threshold and watershed techniques) and deep learning ones (U-Net and R-CNN models). Neverthless as raised by the authors the delimitation of the spheroids contours remains challenging specifically in the case of close or adjacent spheroids. To the best of our knowledge, no work has been proposed in the frame of 3D cell culture on the detection of spheroids issued from the growth of cancer cells [13]. However, in the field of computer vision, object detection is a well established axis. Indeed, several deep learning based architectures have been proposed to address this task such as the YOLOv series [58] and detection transformers [19].

FIGURE 4.2: Our microscopic image acquisition system.

4.3 Materials and Methods

4.3.1 Dataset

Image generation – To generate the image dataset, we first prepared in our laboratory 3D cultures of HeLa cells (cervical cancer cells) following a standard cell proliferation protocol based on BIOMIMESYS technology [76]. Indeed, cervical cancer is currently ranked at the top 4 worldwide cancers within women [80]. For the microscopic image acquisition, we used the ImageXpress system from molecular device company illustrated in Figure 4.2. For this purpose, the microscope confocal magnification has been set to 20-x. In total, 600 z-stack (z=0 to z=50μm) bright-field images with a resolution of 2048 x 2048 pixels have been acquired from a 24-well plate.

Dataset organization – Due to the high amount of generated images (30 000 images), the manual labelling process required to build our training and validation sets for both spheroids detection and nuclei segmentation rapidly became a tedious task for the experts. For this reason, we considered only a subset of z-stack images

namely 50 stacks for the detection and among them 29 stacks for the segmentation. The remaining stacks have been kept for qualitative tests. To ensure a good generalization during the training process of our models, the selected stacks for the labelling have been randomly picked from several wells. Furthermore, from each stack, the experts have labeled one slice image that they have selected along the z-depth according to their own visual perception. More specifically, they have been requested to select the most informative slice in term of spheroid objects for the detection and the nuclei for the segmentation. Following these steps, we created two datasets: 1) a spheroid dataset composed of 50 labeled images with 854 bounding boxes of spheroids. The set has been split into 40 images for training and 10 images for validation. 2) a nuclei dataset composed of 326 spheroid patches (issued from the 29 images) with 1996 delineated nuclei. In this latter case, the set has been split into 249 patches for training and 77 patches for validation. We precise that we made sure that the training patches and validation patches do not come from the same slices. Additionnaly, only separated nuclei with explicit contours have been delineated by the experts.

4.3.2 Methods

Workflow process – As illustrated in Figure 4.3, our framework takes in input a stack of images (Figure 4.3(A)) for which a set of spheroids are detected at the slice level (see traced bounding boxes in Figure 4.3(B)) based on a deep learning model. Each detected spheroid is then cropped and placed into the center of a black background square patch of 512 x 512 pixels (see Figure 4.3(C)). The choice of this latter resolution has been established empirically based on the largest width and height of the spheroids of our dataset. Each spheroid patch is then passed into our deep learning segmentation model which generates a binary mask of identified nuclei (see Figure 4.3(D)). Each binary mask is denoised by removing tiny surfaces according to an empirical threshold. A global binary mask (see Figure 4.3(E)) of the original input image is then generated based on the set of previous masks as well as the spheroid bounding boxes. The resulting spheroid bounding boxes and their nuclei delimited by contours are visualized in Figure 4.3(F). The 3D surface of each segmented nuclei over the stack is then reconstructed as shown in Figure 4.3(G).

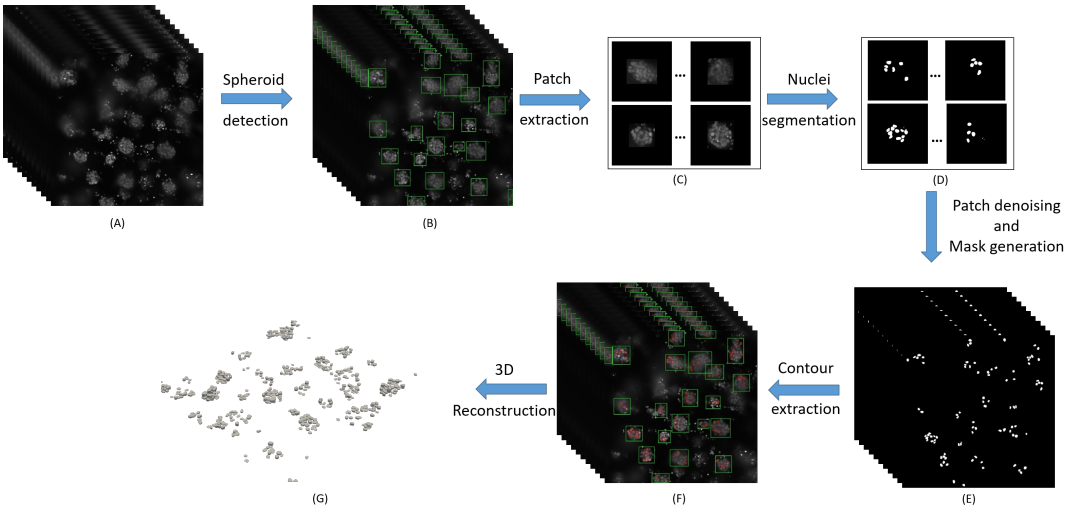

FIGURE 4.3: Workflow process of our hierarchical deep learning framework for nuclei 3D reconstruction.

Deep learning based spheroids detection model – To train our detection model we considered two types of deep architectures namely YOLOv5x [43] [86] and DETR-Resnet50. [19]. Indeed both of these recent architectures have demonstrated a high efficiency over several datasets such as COCO [51] and Pascal [31]. We used the Adam optimizer [46] for both architectures which is the recommended one in the referenced articles. We also used the recommended loss functions namely IOU [74] and hungarian [71] for YOLOv5x and DETR-Resnet50 respectively. The two architectures have been trained following a transfer learning strategy. More specifically, they have been pretrained on the COCO dataset and then trained and validated on our spheroid image dataset producing two detection models.

Deep learning based nuclei segmentation model – To train our segmentation model we considered the U-Net deep architecture [63]. Indeed, this architecture is widely exploited in the field of medical image segmentation [68]. In our case, we customized the architecture by replacing its orginal CNN backbone by a VGG19 [83] [53] one which offers a good tradeoff between the architecture depth and its learning capacity. The model has been trained and validated on our nuclei dataset using Adam optimizer [46] and Jaccard index loss function which is the complement of IOU metric [29].

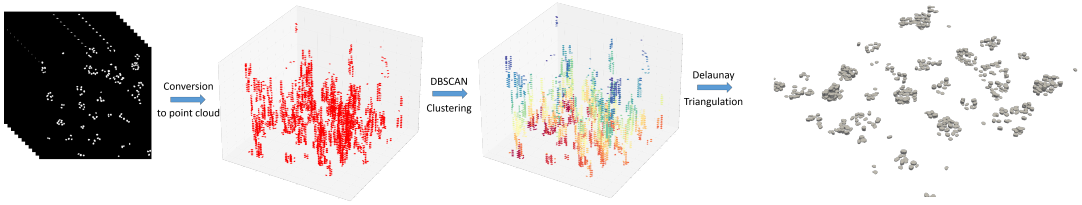

FIGURE 4.4: 3D stack reconstruction pipeline

Unsupervised learning based nuclei 3D reconstruction model – Our built model goes through three main steps (See Figure 4.4) . First, it takes in input the stack of binary masks representing all segmented nuclei and convert it into a 3D point cloud representation. Then, a density-based spatial clustering technique (DBSCAN) [30] is applied in order to identify clusters of 3D points that represent separated nuclei. Finally, the resulting clusters are then used to reconstruct the underlying surfaces of the nuclei using the Delaunay triangulation technique [10].

Evaluation metrics – To evaluate the performance of our detection and segmentation models we adopted standard metrics namely the Precision (Prec), Recall (Rec) and Average Precision (AP) defined as follow:

$$Prec = \frac{TP}{TP + FP} \tag{4.1}$$

$$Rec = \frac{TP}{TP + FN} \tag{4.2}$$

$$AP = \frac{TP}{TP + FP + FN} \tag{4.3}$$

where TP, FP and FN correspond to True Positive, False Positive and False Negative objects. In the case of spheroid objects TP/FP/FN rates are calculated based on an IOU (intersection over union) metric between ground-truth spheroids (i.e. manual annotations of bounding boxes made by the experts) and predicted ones according to several thersholds set in the range [0,5 to 0,9]. The same calculation methodology is applied for estimating the TP/FP/FN rates of nuclei objects. In this latter case, the ground-truth segmentation of nuclei corresponds to binary masks of these objects

issued from the manual delineation of their contours by the experts. For the 3D reconstruction quality evaluation, we limit our experiments in this study on a visual analysis of the shape and the volume of the generated nuclei.

4.4 Experimental study

To evaluate the performance of our framework, we organized our experimental study into 4 sections: the first section is dedicated to the results obtained by our detection models, the second concerns the segmentation model, the third is related to a performance comparison with the direct nuclei segmentation methods from the state of the art and the last section presents some qualitative results.

4.4.1 Spheroids detection performance

Figure 4.5 shows the AP (Average Precision) curves of the two detection models namely YOLOv5x and DETR-Resnet50 obtained on the validation image set (10 images). One can notice that the YOLOv5x has reached the highest performance with notably an AP of 0,848 at an IOU thresholod of 0,5. Nevethless, the DETR model reached also competitive performance. To further improve the performance of the best model namely YOLO we trained it on augmented dataset. More specifically, based on the original training set (40 images) we generated 3 augmented sets: 1) spatial-based augmented set (240 images), 2) texture-based augmented set (200 images) and 3) combined augmented set (400 images). For the spatial augmentation, we applied 3 rotations (90, 180 and 270 degrees) and 2 flips (horizontal and vertical). For the texture augmentation, we applied 2 levels of contrast and brightness variations. The combined augmentation corresponds to the merge of all the afformentioned augmentations. Figure 4.6 shows the obtained AP curves on the validation set for each augmentation scenario together with the original train set (without augmentation). The figure shows that the combined augmentation has permitted to gain 4,4% more in term of AP reaching a score of 0,892 at IOU threshold equal to 0,5. Table 4.1 sumarizes for this latter scenario the TP/FP/FN rates as well as Prec and Rec metrics calculated on the basis of an IOU threshold set to 0,5. The table shows the high performance of the trained detection model.

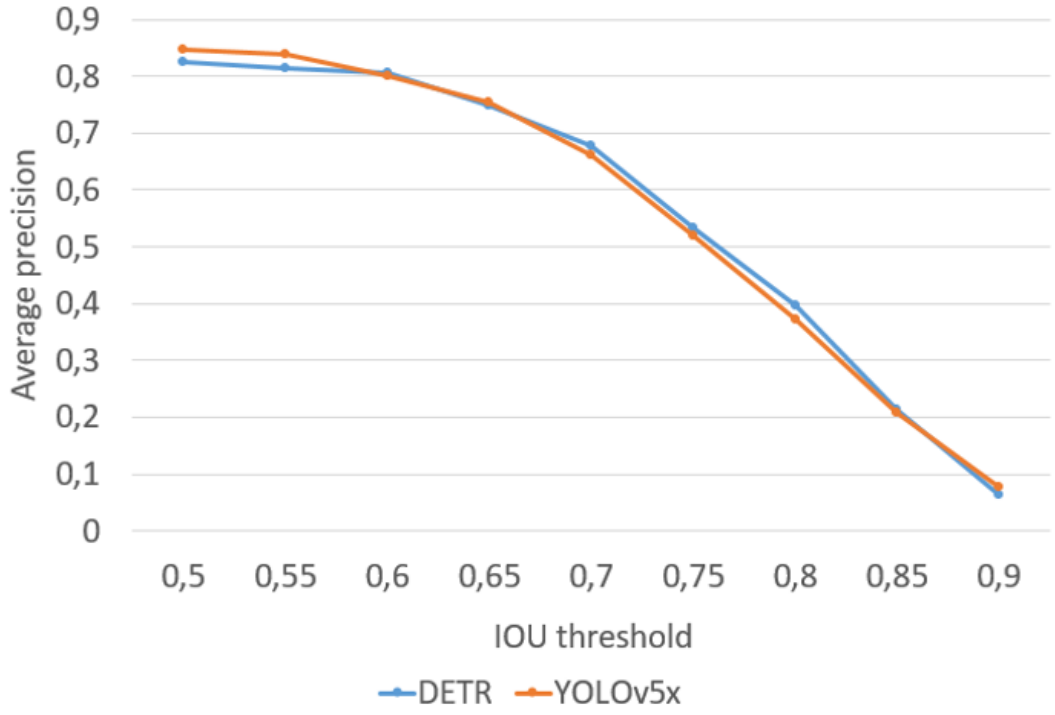

FIGURE 4.5: Performance of the spheroids detection models obtained on the validation set.

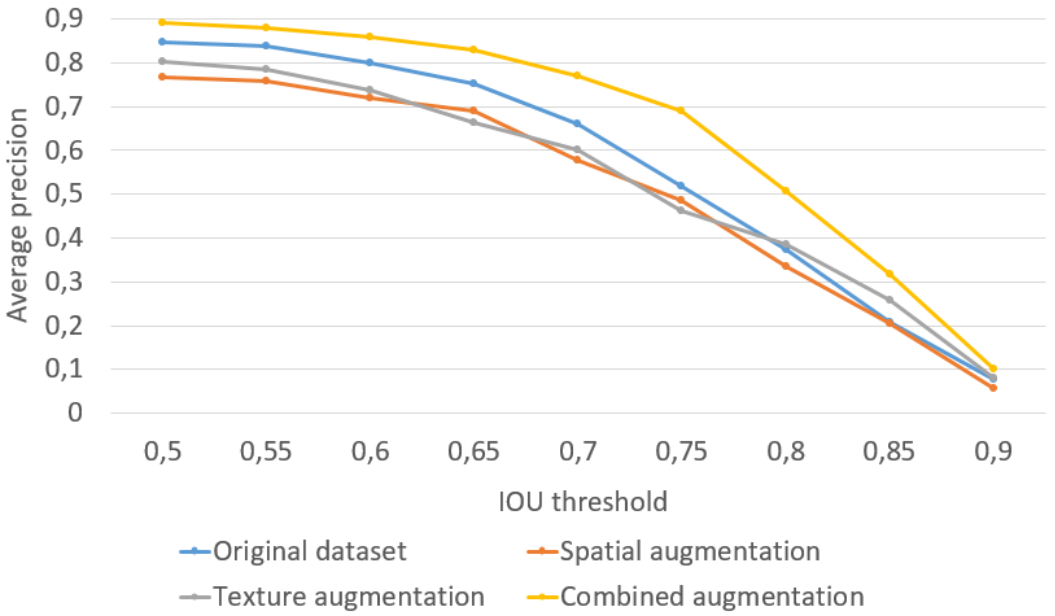

FIGURE 4.6: Performance of four YOLOv5x-based spheroid detection models obtained on the validation set. The models are trained following four scenarios of data augmentation.

TP	FP	FN	Prec	Rec
157	012	007	0,929	0,957

TABLE 4.1: Performance of the YOLOv5x-based spheroids detection model obtained on the validation set with $IOU_{@0,5}$. Model trained on the combined augmented set (400 images).

Augmentation	Prec	Rec	AP
None	0,535	0,616	0,401
Texture	**0,649**	0,369	0,307
Spatial	0,594	**0,723**	**0,484**
Combined	0,620	0,608	0,443

TABLE 4.2: Performance of nuclei segmentation models obtained on the validation set of spheroid patches with $IOU_{@0,5}$.

4.4.2 Nuclei segmentation performance

Similarly to the detection model, we have trained our segmentation model on 4 training sets including the original training set (249 patches) and 3 augmented sets following the same strategies indicated in the previous section, i.e. spatial (1494 patches), texture (1245 patches) and combined (2490 patches) augmentations. Table 4.2 summarizes the obtained performance by our models on the validation set (77 patches) for each training scenario and with an IOU threshold set to 0,5. The table shows that the highest performance are obtained by the model trained on the spatial-based augmentation set. The model has reached a Rec score of 0,723 indicating that a weak number of ground-truth nuclei have been missed by it. However, the Prec score of the model is low indicating the high number of detected FP nuclei. In fact, after visually analyzing these FP by the experts it was found that several objects among them are corresponding to true nuclei. Figure 4.7 highlights this observation through a compartive example between a ground-truth nuclei segmentation vs. predicted one on the same spheroid patch. Hence, the nuclei ground-truth of the validation set has been updated by adding correctly predicted nuclei by our model. Following this update, the number of ground-truth nuclei has increased from 301 to 519. In addition, the Prec and the AP have increased to 0,911 and 0,760 respectively.

4.4.3 Segmentation performance comparison: our framework vs. state of the art direct segmentation methods

We considered two methods from the state of the art: Cellpose [72] and StarDist [67]. The Cellpose is a generalized segmentation method that is designed and trained to efficiently segment a population of objects with repetitive shapes whatever their natures (cells, neurons, etc.) and their geometric forms. The StarDist is a nuclei segmentation method that aims to delimit contours of objects (nuclei cells) having

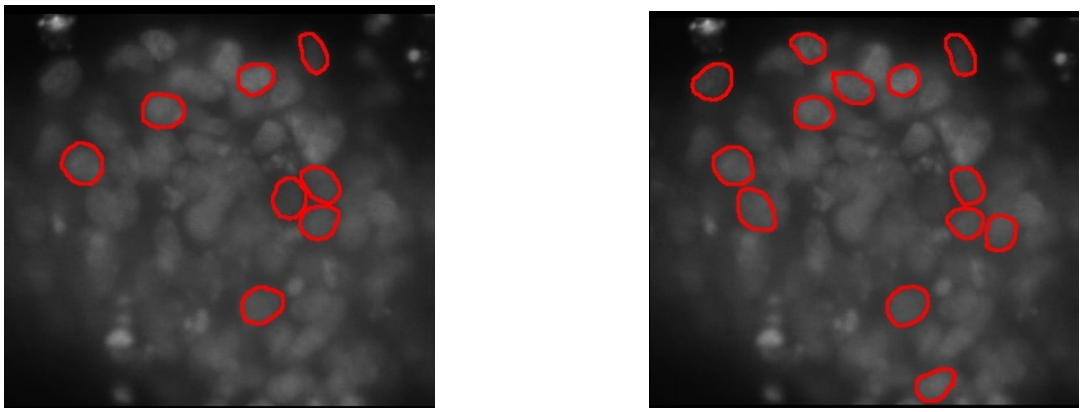

(A) (B)

FIGURE 4.7: Manually labeled nuclei (a) vs Predicted nuclei (b).

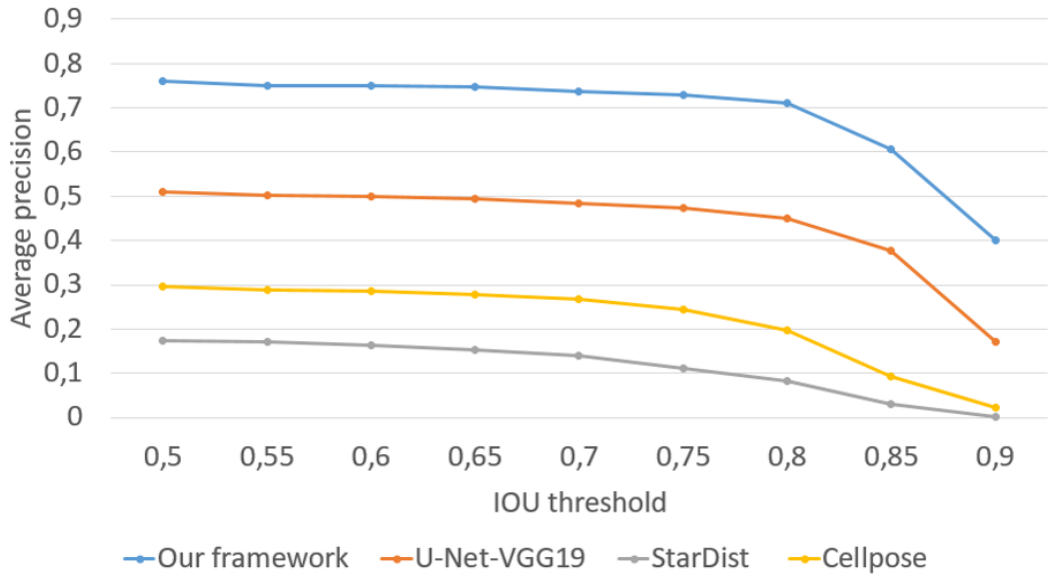

FIGURE 4.8: Segmentation performance comparison between our framework and state of the art methods obtained on the validation set.

a convex shape. Both of the methods are built on a U-Net architecture. To evaluate these two methods on our dataset: i) The StarDist model pretrained on the Bowl 2018 nuclei dataset has been fine-tuned on the slice images of our training set. To this end, ground-truth global masks have been generated from shperoid patches. ii) The Cellpose method has not been trained since it offers a generalized nuclei segmentation model trained on several combined microscopy datasets including the Bowl 2018 nuclei dataset. However, the model has been parametrized by setting up its nuclei diameter option according to our dataset nuclei. The two models have been tested on our updated nuclei validation set (519 nuclei). In addition, we trained a U-Net

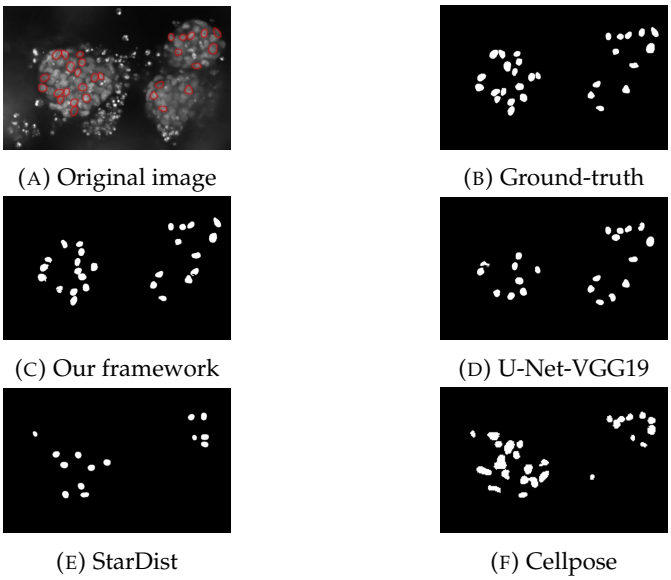

(A) Original image (B) Ground-truth

(C) Our framework (D) U-Net-VGG19

(E) StarDist (F) Cellpose

FIGURE 4.9: Qualitative results of segmentation obtained by our framework and state of the art methods.

with a VGG19 backbone directly on the slice images and validated it on the same set (519 nuclei). Figure 4.8 shows the AP curves of the 3 models compared to the AP curve of our framework. One may observe that our framework outperformed the three methods. More specifically, it has reached an AP of 0,76 at an IOU set to 0,5. We can observe also that the StarDist model has the lowest AP (0,174) although it has been trained (fine-tuned) on our nuclei training set. This result was expected due to the unadapted criterion to our data on which the architecture was designed namely the convexity of the nuclei shape. The Cellpose reached a better AP (0,295) than StarDist although it has been tested directly on the validation set without training. However its score remains low in comparison with our framework showing again the diffculty of segmenting the nuclei of our data by exploiting a direct segmentation approach. Finally, this latter observation is confirmed with the U-Net-VGG19 model that has been trained on the slice images and reached an AP of 0,509. These results demonstrate the contribution of our analysis strategy which first detect the spheroids and then segment their nuclei. Moreover, as illustrated in Figure 4.9 our strategy permits to cover all the spheroids and thus detect nuclei in each of them which is not guaranteed with the direct segmentation methods.

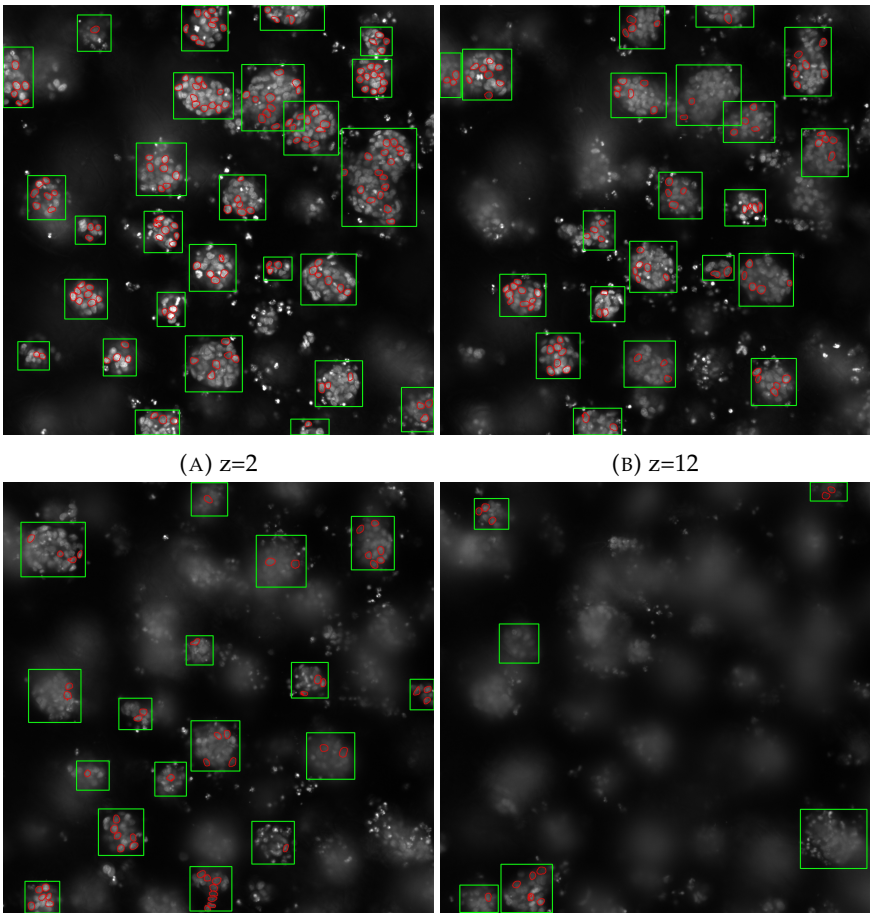

(A) z=2 (B) z=12

(C) z=26 (D) z=48

FIGURE 4.10: Qualitative result obtained by our framework on a blind stack (not exploited in the training and validation sets) along several z-depth.

4.4.4 Qualitative results

Generalization of detection and segmentation models – To analyze the generalization potential of our framework as well as its z-depth sensitivity, we have tested it on several blind z-stacks (stacks that haven't been exploited in the training/validation sets). Figure 4.10 illustrates some qualitative results obtained on one z-stack with z= 3, 12, 26 and 48. One can observe that our framework has succeeded to detect almost all the spheroids and segment some of their nuclei whatever the slice depth. We also observe that the framework offers a good robustness against noise present in the slices. Indeed, all the identified objects either from the detection model or from the segmentation model are relevant objects.

3D Reconstruction – In Figure 4.11(A) we show the result of our reconstruction model on a blind stack (not used in the training and validation process). In order

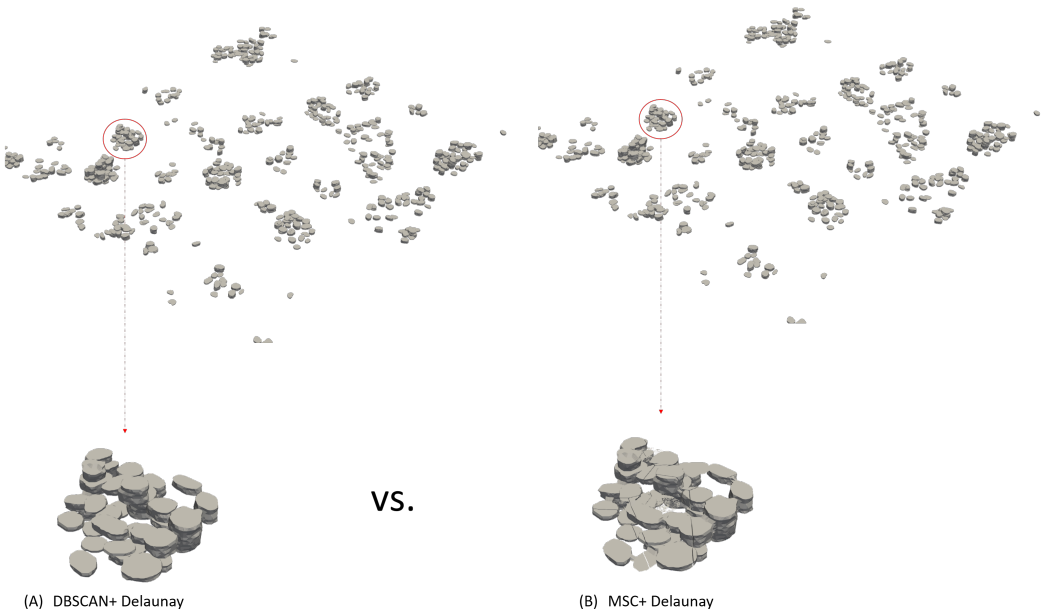

FIGURE 4.11: Comparison between two 3D reconstruction mesh results formed with two different clustering methods (DBSCAN and MSC) with the Delaunay triangulation

to analyse the impact of the clustering technique on the resulting reconstruction, we have replaced DBSCAN by the Mean Shift Clustering (MSC) [84]. The reconstruction results obtained on the same blind stack is shown in Figure 4.11(B). One can notice that from a global point of view the reconstruction model is able to generate surfaces of several objects whatever is the exploited clustering technique. Nevertheless, as illustrated in the Figure, a special focus on a small area of the 3D view permits to highlight the efficiency of the DBSCAN compared to the MSC. More specifically, we can observe that the 3D nuclei surfaces generated from MSC are not well separated, are cracked, and include noise. To understand the reasons of this result, we have investigated the correlation between the identified clusters and the binary masks of the segmented nuclei. Figure 4.12 illustrates an example of this correlation on a small patch extracted from one slice image. One may observe that, contrary to the MSC, the DBSCAN is able to correctly identify the nuclei objects since each one of them is represented by one separated cluster.

(A) MSC (B) DBSCAN

FIGURE 4.12: MSC vs DBSCAN clustering results

4.5 Conclusion

In this study, we have presented a hierarchical deep learning framework for the nuclei 3D reconstruction. For this purpose we prepared a dataset of bright-field microscopic images composed of 854 manually anotated spheroids and 1996 delineated nuclei by the experts. The two trained CNN models namely yolov5x for the detection and Unet-VGG19 for the segmentation have shown high performance on our validation set by reaching an AP (Average Precision) scores of 0,892 and 0,76 respectively. Several findings have been revealed in our study: 1) combined augmentations based on spatial and texture transformations have permitted to improve the precision of the detection model while only spatial transformations permitted to improve the precision of the segmentation model. 2) segmentation model trained on weakly labeled data succeeded to segment nuclei that have not been annotated by the experts. 3) hierarchical analysis (spheroids detection then nuclei segmentation) permitted to improve the segmentation quality compared to direct segmentation methods from the state of the art. 4) training the models on the most informative slices (only one slice picked from each stack) permitted to ensure a good generalization potential of these models, a result that has been confirmed qualitatively on several stacks along the z-depth. 5) The Delaunay triangulation applied on segmented nuclei achieved a better 3D visual representation when using DBSCAN clustering.

Chapter 5

Conclusion and Perspectives

5.1 Summary

During these 3 years of research we dedicated our work into finding answers and possibilities to achieve a 3D reconstruction of nuclei from 2D microscopic images acquired from 3D cell culture. Coming from an engineering background, it was a challenge to work in a biological field and be introduced to cell culture and microscopy. It's very interesting to discover the cell structure and understand the importance of working in the cell environment to biologists.

Indeed, working with cell culture can help experts in different tasks. As an example and one of the most important and crucial study in the scientific community is drug discovery. As the process of drug discovery is evolving, cell culture and microscopy techniques are also evolving. Usually biologists are more familiar with 2D cell culture since it is low cost and more flexible and easy to manipulate and work with. The acquired microscopic images are easy to read and analyse. However 2D cell culture does not represent the human cells and does not mimic their functions. To this extent, 3D cell culture was introduced, a more realistic procedure to human cell environment however more complex. Indeed, 3D cell culture are known to be developed in a translucent culture which introduce several artifacts in the generated microscopic images such as blurred objects, overlapping objects,etc..

We needed to develop automatic methods to help biologists conduct their analysis and to save them a considerable amount of time as automatic systems can analyse thousands of data images in a short amount of time.

To start understanding our contribution to such an interesting and important

scientific study, we wanted to discover and test the available softwares that are used to perform automatic analysis. We put in place an evaluation of several machine learning classifiers using different combinations to test the efficiency and robustness of these methods for the segmentation task (nuclei). We came up with the conclusion that even though these methods can help in segmenting specific areas, they fail in separating the overlapped nuclei inside the z-stack of 2D images acquired from 3D cell culture.

To overcome this limit, we developped a workflow based on several machine learning processes and more advanced architectures based on deep learning. The idea is to start detecting all the spheroids in the microscopic image. After detecting all the spheroids, we segmented the most visible, ellipsoidal shaped nuclei inside each spheroid. And, as we are working with 3D cell culture meaning in a stack of 2D microscopic images, we reconstructed the segmented nuclei inside the stack to have the 3d representation of the full environment. The deep learning methods, Yolov5 and Unet+Vgg19 succeeded respectively in first detecting most of the spheroids in the microscopic images and outperformed the manual segmentation of the nuclei in each spheroid.

In the end, we had the 3D reconstruction of the nuclei from the segmented microscopic images. This is a huge advancement as it can help biologists study the morphological and physiological changes with the drug injected in the cell culture.

5.2 Future Work

Although our obtained 3D reconstruction result is promising and a great step in the analysis of 3D cell culture, it opens new door for further improvements. Indeed different applications may be added to the system to either improve the learning performances or help further in the analysis.

Models improvements– Deep learning algorithms are data driven. Indeed, as we can see in Figure 5.1, the performance is affected as we input more data to the system and in our case more images for the detection and segmentation problems. However, the lack of manual segmentation makes it difficult to train our systems on hundreds

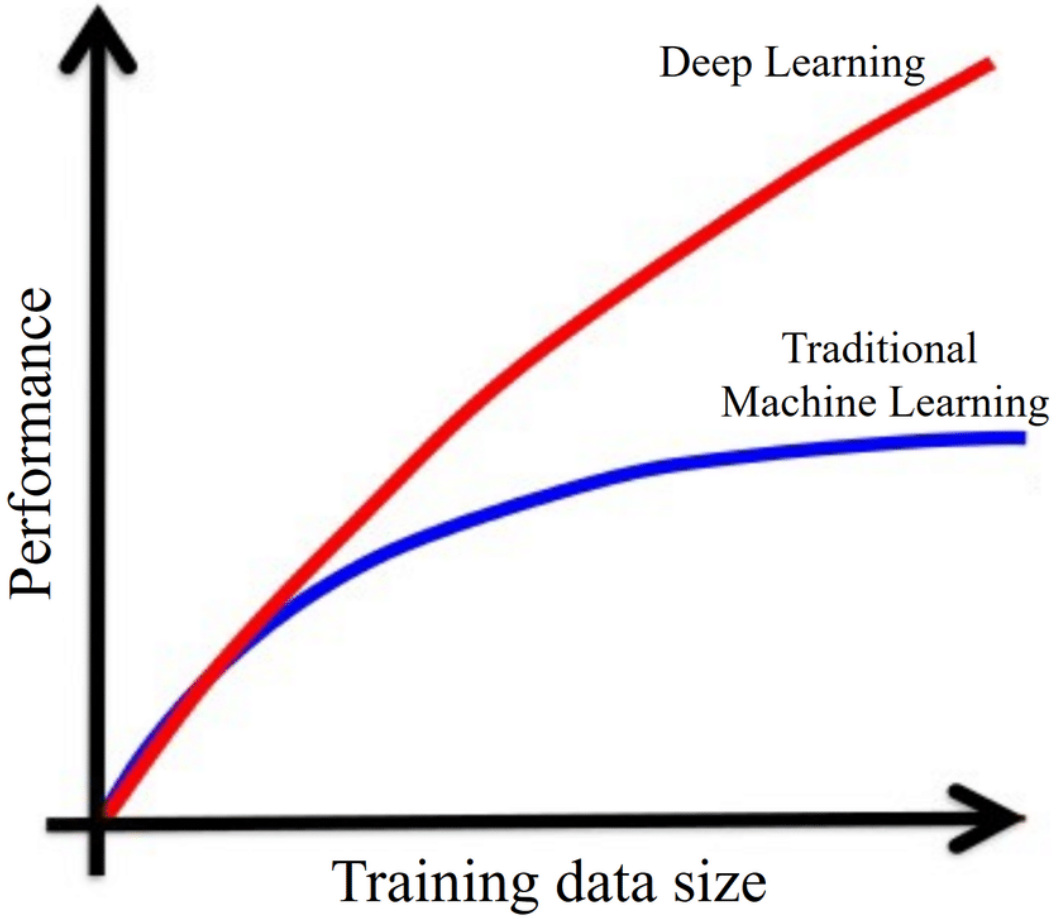

FIGURE 5.1: The correlation between the algorithms performance and the amount of data [3]

of images. The community is in need of labeled data and it will be a great first step to prepare a valuable amount of data that can benifit the scientific comunity and may help in developing in the near future some automatic labeling tools. To this extent, an intiative could be made to create an online plateform for biologists to gather labeled data images and thus creating an open source dataset for scientists and researchers. An annotation tool can be developed that automatically drops the manually annoted image in an online cloud.

Automatic Morphological Analysis– The 3D reconstruction is very important to biologists, however, it is also crucial for them to have morphological measurements related to the nuclei. Developing an automatic method could help to determine several information on each nucleus in the 3D image such as its area or volume and

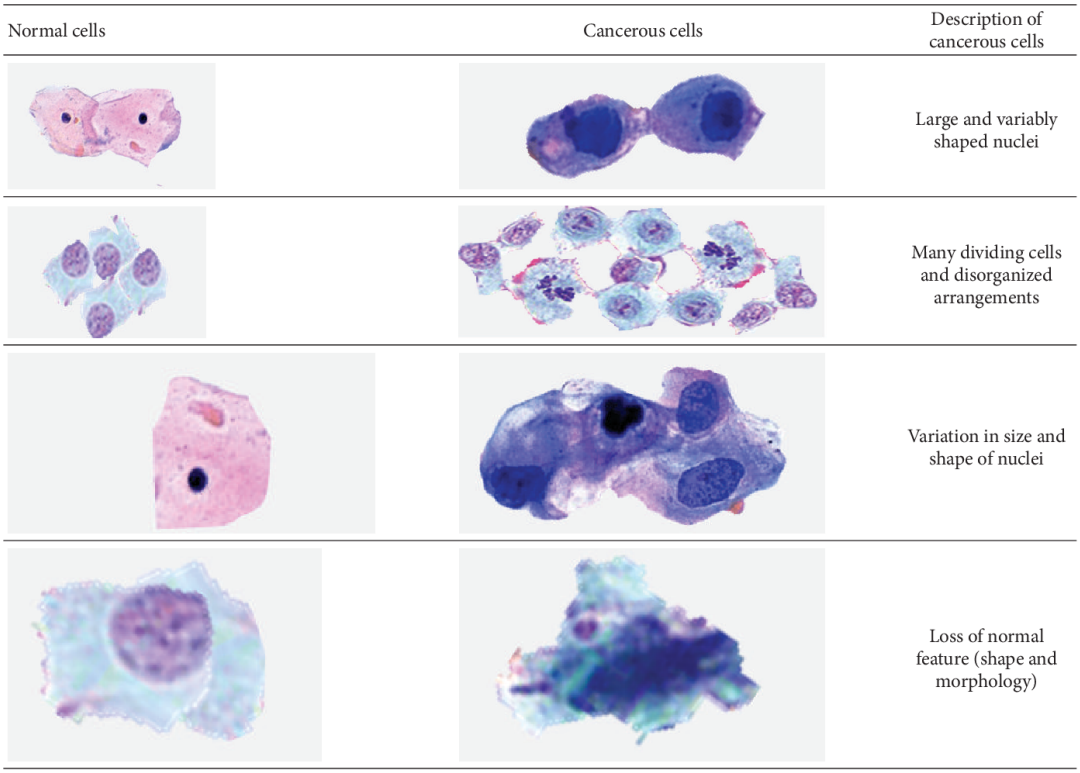

FIGURE 5.2: Comparison between a normal and cancerous cell structure

dimensions such as diameter radius, circumference and height. Figure 5.2 represents the biological and morphological aspects between normal and cancerous cells and nuclei [47]. Such methods may also indicate the number of nuclei inside the 3D image. A deep learning algorithm could also improve the analysis by trying to compare the measurements between the different periods of proliferation and the drug effect on the nuclei over time. A further step can also be added that consists of automatically locating the nuclei that are still intact and the ones that died over time. This application would be an efficient tool to evaluate the changes that occur during a drug test process.

Generalised Algorithm– The study could also be expanded to different components such as cells, membrane, neurones,etc. A generalised algorithm could be developed that includes several types of analysis on different components and types of microscopy. This future work could be a great help for biologists to analyse any type of data and thus being able to conduct their interpretation faster through a single system (Figure 5.3). A software could be developed that allows the user to choose

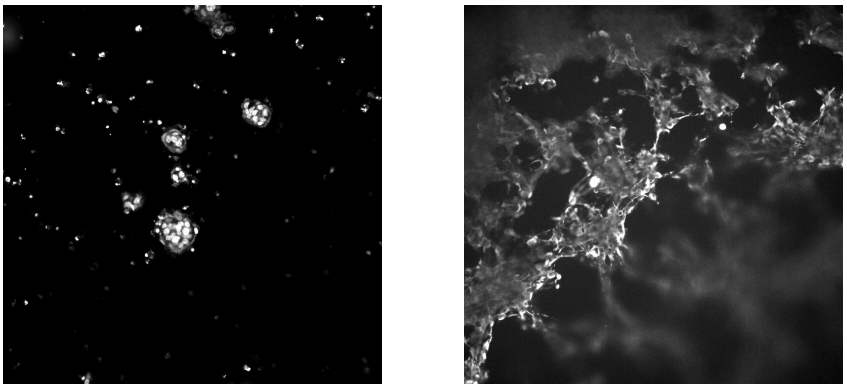

(A) Microscopic image of nuclei (B) Microscopic image of neurons

FIGURE 5.3: Different types of microscopic images

the type of images and cell structure that he wants to analyse. Then the system will automatically select the best model that works well on the type of images provided by the user.

Quantitative 3D Analysis– A quantitative 3D analysis could be also a great evaluation for the 3D reconstruction. A 3D reconstruction benchmark could be established by first reconstructing manually the nuclei and specifying evaluation metrics that can compare the manual and the automated reconstruction.

Another application may be added to the 3D reconstruction application by generating microscopic images from different angles. This experimentation allows to generate the complete 3D reconstruction of the spherical-like shaped nuclei and thus tracking the changes that occurs during a drug testing process on all the sides of the nuclei.

To conclude, this work was very rewarding as I personally evolved by widening my knowledge and opening myself to a new horizon which is the biological field. It helped me understand the importance of the studies conducted in this domain. And I'm glad we achieved a progress that can help the community advance in their research. I also discovered the importance of artificial intelligence in the communities as it can be a helpful tool in the technological advancement in all fields and as Jeff Bezos said: "We're at the beginning of a golden age of AI. Recent advancements have already led to invention that previously lived in the realm of science fiction —

and we've only scratched the surface of what's possible".

Bibliography

[1] *2D vs 3D - Creative Biolabs*. en-us. URL: https://www.creative-biolabs.com/adc/2d-vs-3d.htm (visited on 09/21/2022).

[2] Yousef Al-Kofahi et al. "A deep learning-based algorithm for 2-D cell segmentation in microscopy images". eng. In: *BMC bioinformatics* 19.1 (Oct. 2018), p. 365. ISSN: 1471-2105. DOI: 10.1186/s12859-018-2375-z.

[3] Zaid Alyafeai and Lahouari Ghouti. "A Fully-Automated Deep Learning Pipeline for Cervical Cancer Classification". In: *Expert Systems with Applications* 141 (Sept. 2019), p. 112951. DOI: 10.1016/j.eswa.2019.112951.

[4] Marc Arbyn et al. "Estimates of incidence and mortality of cervical cancer in 2018: a worldwide analysis". eng. In: *The Lancet. Global Health* 8.2 (Feb. 2020), e191–e203. ISSN: 2214-109X. DOI: 10.1016/S2214-109X(19)30482-6.

[5] Ignacio Arganda-Carreras et al. "Trainable Weka Segmentation: a machine learning tool for microscopy pixel classification". eng. In: *Bioinformatics (Oxford, England)* 33.15 (Aug. 2017), pp. 2424–2426. ISSN: 1367-4811. DOI: 10.1093/bioinformatics/btx180.

[6] *Background*. en. Publication Title: Comprehensive Cervical Cancer Control: A Guide to Essential Practice. 2nd edition. World Health Organization, 2014. URL: https://www.ncbi.nlm.nih.gov/books/NBK269623/ (visited on 09/13/2022).

[7] Brendon M. Baker and Christopher S. Chen. "Deconstructing the third dimension: how 3D culture microenvironments alter cellular cues". eng. In: *Journal of Cell Science* 125.Pt 13 (July 2012), pp. 3015–3024. ISSN: 1477-9137. DOI: 10.1242/jcs.079509.

[8] D. Baltissen et al. "Comparison of segmentation methods for tissue microscopy images of glioblastoma cells". In: *2018 IEEE 15th International Symposium on Biomedical Imaging (ISBI 2018)*. Washington, DC: IEEE, Apr. 2018, pp. 396–399. ISBN: 978-1-5386-3636-7. DOI: 10.1109/ISBI.2018.8363601. URL: https://ieeexplore.ieee.org/document/8363601/ (visited on 09/09/2022).

[9] *BIOMIMESYS® 3D cell culture products - HCS Pharma*. URL: https://hcs-pharma.com/biomimesys/ (visited on 09/09/2022).

[10] Boris Delaunay. "Sur la sphere vide". In: *Bull. Acad. Science USSR VII: Class. Sci. Mat* 17.8 (Aug. 1934), pp. 793–800. ISSN: 01628828. (Visited on 05/11/2022).

[11] Leo Breiman. "Random Forests". en. In: *Machine Learning* 45.1 (Oct. 2001), pp. 5–32. ISSN: 1573-0565. DOI: 10.1023/A:1010933404324. URL: https://doi.org/10.1023/A:1010933404324 (visited on 09/09/2022).

[12] Federica Bubba et al. "A chemotaxis-based explanation of spheroid formation in 3D cultures of breast cancer cells". eng. In: *Journal of Theoretical Biology* 479 (Oct. 2019), pp. 73–80. ISSN: 1095-8541. DOI: 10.1016/j.jtbi.2019.07.002.

[13] Federica Bubba et al. "A chemotaxis-based explanation of spheroid formation in 3D cultures of breast cancer cells". en. In: *Journal of Theoretical Biology* 479 (Oct. 2019), pp. 73–80. ISSN: 00225193. DOI: 10.1016/j.jtbi.2019.07.002. URL: https://linkinghub.elsevier.com/retrieve/pii/S0022519319302796 (visited on 03/08/2022).

[14] Wilhelm Burger and Mark J. Burge. "ImageJ". In: *Digital Image Processing*. Series Title: Texts in Computer Science. London: Springer London, 2016, pp. 23–35. ISBN: 978-1-4471-6683-2 978-1-4471-6684-9. DOI: 10.1007/978-1-4471-6684-9_2. URL: http://link.springer.com/10.1007/978-1-4471-6684-9_2 (visited on 09/09/2022).

[15] Juan C. Caicedo et al. "Nucleus segmentation across imaging experiments: the 2018 Data Science Bowl". en. In: *Nature Methods* 16.12 (Dec. 2019), pp. 1247–1253. ISSN: 1548-7091, 1548-7105. DOI: 10.1038/s41592-019-0612-7. URL: http://www.nature.com/articles/s41592-019-0612-7 (visited on 03/10/2022).

[16] *Cancer*. en. URL: https://www.who.int/health-topics/cancer (visited on 09/09/2022).

[17] *Cancer Data and Statistics | CDC*. en-us. June 2022. URL: https://www.cdc.gov/cancer/dcpc/data/index.htm (visited on 09/09/2022).

[18] *Cancer Facts & Figures 2021 | American Cancer Society*. en. URL: https://www.cancer.org/research/cancer-facts-statistics/all-cancer-facts-figures/cancer-facts-figures-2021.html (visited on 09/09/2022).

[19] Nicolas Carion et al. "End-to-End Object Detection with Transformers". en. In: *Computer Vision – ECCV 2020*. Ed. by Andrea Vedaldi et al. Vol. 12346. Series Title: Lecture Notes in Computer Science. Cham: Springer International Publishing, 2020, pp. 213–229. ISBN: 978-3-030-58451-1 978-3-030-58452-8. DOI: 10.1007/978-3-030-58452-8_13. URL: https://link.springer.com/10.1007/978-3-030-58452-8_13 (visited on 03/10/2022).

[20] *Cellular Imaging Systems, ImageXpress High-Content Imaging & Analysis, Digital & Confocal Microscopy | Molecular Devices*. URL: https://www.moleculardevices.com/products/cellular-imaging-systems?cmp=7010g000000nNEc&utm_source=AdWords&utm_medium=cpc&utm_campaign=IMG-Brand_Regional&utm_adgroup={adgroup}&utm_location=9055145&utm_keyword=%2Bimagexpress%20molecular%20devices&utm_device=c&utm_devicemodel=&utm_placement=&utm_adpostion=&utm_target=&utm_network=g&utm_creative=433998034951&gclid=EAIaIQobChMIi878ibam-gIV1eN3Ch01hwENEAAYASAAEgK4UfD_BwE (visited on 09/21/2022).

[21] *Cervical cancer - Symptoms and causes*. en. URL: https://www.mayoclinic.org/diseases-conditions/cervical-cancer/symptoms-causes/syc-20352501 (visited on 09/21/2022).

[22] *Cervical Cancer | Patient Care*. URL: https://weillcornell.org/services/obstetrics-and-gynecology/gynecologic-oncology/conditions-we-treat/cervical-cancer (visited on 09/21/2022).

[23] *Cervical Cancer Survival Rates | Cancer 5 Year Survival Rates*. URL: https://www.cancer.org/cancer/cervical-cancer/detection-diagnosis-staging/survival.html (visited on 09/15/2022).

[24] Office of the Commissioner. *The Drug Development Process*. en. Publisher: FDA. Feb. 2020. URL: https://www.fda.gov/patients/learn-about-drug-and-device-approvals/drug-development-process (visited on 09/09/2022).

[25] *DAPI staining improved for quantitative cytofluorometry | SpringerLink*. URL: https://link.springer.com/article/10.1007/BF00489783 (visited on 09/12/2022).

[26] Yi De Xie. "Multi-pixels Classification for nuclei segmentation in digital pathology based on deep machine learning". In: *Journal of Physics: Conference Series* 1087 (Sept. 2018), p. 062030. ISSN: 1742-6588, 1742-6596. DOI: 10.1088/1742-6596/1087/6/062030. URL: https://iopscience.iop.org/article/10.1088/1742-6596/1087/6/062030 (visited on 09/09/2022).

[27] Jayanta Debnath and Joan S. Brugge. "Modelling glandular epithelial cancers in three-dimensional cultures". eng. In: *Nature Reviews. Cancer* 5.9 (Sept. 2005), pp. 675–688. ISSN: 1474-175X. DOI: 10.1038/nrc1695.

[28] Aparna Dravid U. and Nirmal Mazumder. "Types of advanced optical microscopy techniques for breast cancer research: a review". en. In: *Lasers in Medical Science* 33.9 (Dec. 2018), pp. 1849–1858. ISSN: 0268-8921, 1435-604X. DOI: 10.1007/s10103-018-2659-6. URL: http://link.springer.com/10.1007/s10103-018-2659-6 (visited on 09/12/2022).

[29] Tom Eelbode et al. "Optimization for Medical Image Segmentation: Theory and Practice When Evaluating With Dice Score or Jaccard Index". In: *IEEE Transactions on Medical Imaging* 39.11 (Nov. 2020), pp. 3679–3690. ISSN: 0278-0062, 1558-254X. DOI: 10.1109/TMI.2020.3002417. URL: https://ieeexplore.ieee.org/document/9116807/ (visited on 03/25/2022).

[30] Martin Ester, Hans-Peter Kriegel, and Xiaowei Xu. "A Density-Based Algorithm for Discovering Clusters in Large Spatial Databases with Noise". en. In: (), p. 6.

[31] Mark Everingham et al. "The Pascal Visual Object Classes (VOC) Challenge". en. In: *International Journal of Computer Vision* 88.2 (June 2010), pp. 303–338. ISSN: 0920-5691, 1573-1405. DOI: 10.1007/s11263-009-0275-4. URL: http://link.springer.com/10.1007/s11263-009-0275-4 (visited on 03/14/2022).

[32] Jacques Ferlay et al. “Cancer statistics for the year 2020: An overview”. en. In: (), p. 12.

[33] Dmytro Fishman et al. *Segmenting nuclei in brightfield images with neural networks*. en. preprint. Bioinformatics, Sept. 2019. DOI: 10.1101/764894. URL: http://biorxiv.org/lookup/doi/10.1101/764894 (visited on 09/09/2022).

[34] Aslı Gençtav, Selim Aksoy, and Sevgen Önder. “Unsupervised segmentation and classification of cervical cell images”. en. In: *Pattern Recognition* 45.12 (Dec. 2012), pp. 4151–4168. ISSN: 00313203. DOI: 10.1016/j.patcog.2012.05.006. URL: https://linkinghub.elsevier.com/retrieve/pii/S0031320312002191 (visited on 09/09/2022).

[35] *Glossary: Three Rs principle (in animal experimentation)*. URL: https://ec.europa.eu/health/scientific_committees/opinions_layman/en/non-human-primates/glossary/tuv/three-rs-principle.htm (visited on 09/15/2022).

[36] Istvan Grexa et al. “SpheroidPicker for automated 3D cell culture manipulation using deep learning”. en. In: *Scientific Reports* 11.1 (Dec. 2021), p. 14813. ISSN: 2045-2322. DOI: 10.1038/s41598-021-94217-1. URL: http://www.nature.com/articles/s41598-021-94217-1 (visited on 03/10/2022).

[37] Ola Habanjar et al. “3D Cell Culture Systems: Tumor Application, Advantages, and Disadvantages”. en. In: *International Journal of Molecular Sciences* 22.22 (Nov. 2021), p. 12200. ISSN: 1422-0067. DOI: 10.3390/ijms222212200. URL: https://www.mdpi.com/1422-0067/22/22/12200 (visited on 03/08/2022).

[38] Mark Hall et al. “The WEKA data mining software: an update”. en. In: *ACM SIGKDD Explorations Newsletter* 11.1 (Nov. 2009), pp. 10–18. ISSN: 1931-0145, 1931-0153. DOI: 10.1145/1656274.1656278. URL: https://dl.acm.org/doi/10.1145/1656274.1656278 (visited on 09/09/2022).

[39] *HeLa cells 50 years on: the good, the bad and the ugly | Nature Reviews Cancer*. URL: https://www.nature.com/articles/nrc775 (visited on 09/12/2022).

[40] *High-Content Screening - an overview | ScienceDirect Topics*. URL: https://www-sciencedirect-com.ressources-electroniques.univ-lille.fr/

topics/medicine-and-dentistry/high-content-screening (visited on 09/12/2022).

[41] Reka Hollandi et al. "Nucleus segmentation: towards automated solutions". en. In: *Trends in Cell Biology* (Jan. 2022), S0962892421002518. ISSN: 09628924. DOI: 10.1016/j.tcb.2021.12.004. URL: https://linkinghub.elsevier.com/retrieve/pii/S0962892421002518 (visited on 03/10/2022).

[42] *Introduction to Cell Culture - FR*. fr. URL: https://www.thermofisher.com/fr/fr/home/references/gibco-cell-culture-basics/introduction-to-cell-culture.html (visited on 09/12/2022).

[43] Glenn Jocher. *Yolov5 Ultralytics*. URL: https://github.com/ultralytics/yolov5 (visited on 03/15/2022).

[44] Marta Kapałczyńska et al. "2D and 3D cell cultures – a comparison of different types of cancer cell cultures". In: *Archives of Medical Science : AMS* 14.4 (June 2018), pp. 910–919. ISSN: 1734-1922. DOI: 10.5114/aoms.2016.63743. URL: https://www.ncbi.nlm.nih.gov/pmc/articles/PMC6040128/ (visited on 03/08/2022).

[45] Marta Kapałczyńska et al. "2D and 3D cell cultures – a comparison of different types of cancer cell cultures". In: *Archives of Medical Science : AMS* 14.4 (June 2018), pp. 910–919. ISSN: 1734-1922. DOI: 10.5114/aoms.2016.63743. URL: https://www.ncbi.nlm.nih.gov/pmc/articles/PMC6040128/ (visited on 09/15/2022).

[46] Diederik P. Kingma and Jimmy Ba. *Adam: A Method for Stochastic Optimization*. Jan. 29, 2017. arXiv: 1412.6980[cs]. URL: http://arxiv.org/abs/1412.6980 (visited on 02/10/2023).

[47] Rajesh Kumar, Rajeev Srivastava, and Subodh Srivastava. "Detection and Classification of Cancer from Microscopic Biopsy Images Using Clinically Significant and Biologically Interpretable Features". In: *Journal of Medical Engineering* 2015 (2015).

[48] Sigrid A. Langhans. "Three-Dimensional in Vitro Cell Culture Models in Drug Discovery and Drug Repositioning". In: *Frontiers in Pharmacology* 9 (Jan. 2018),

p. 6. ISSN: 1663-9812. DOI: 10.3389/fphar.2018.00006. URL: http://journal.frontiersin.org/article/10.3389/fphar.2018.00006/full (visited on 09/09/2022).

[49] Jeff W. Lichtman and José-Angel Conchello. "Fluorescence microscopy". eng. In: *Nature Methods* 2.12 (Dec. 2005), pp. 910–919. ISSN: 1548-7091. DOI: 10.1038/nmeth817.

[50] Sean Lin et al. "Image-based high-content screening in drug discovery". eng. In: *Drug Discovery Today* 25.8 (Aug. 2020), pp. 1348–1361. ISSN: 1878-5832. DOI: 10.1016/j.drudis.2020.06.001.

[51] Tsung-Yi Lin et al. "Microsoft COCO: Common Objects in Context". In: *Computer Vision – ECCV 2014*. Ed. by David Fleet et al. Cham: Springer International Publishing, 2014, pp. 740–755. ISBN: 978-3-319-10602-1.

[52] Chenyi Ling et al. "Analyzing U-Net Robustness for Single Cell Nucleus Segmentation from Phase Contrast Images". en. In: *2020 IEEE/CVF Conference on Computer Vision and Pattern Recognition Workshops (CVPRW)*. Seattle, WA, USA: IEEE, June 2020, pp. 4157–4163. ISBN: 978-1-72819-360-1. DOI: 10.1109/CVPRW50498.2020.00491. URL: https://ieeexplore.ieee.org/document/9150701/ (visited on 03/10/2022).

[53] Fangyu Liu and Linbing Wang. "UNet-based model for crack detection integrating visual explanations". en. In: *Construction and Building Materials* 322 (Mar. 2022), p. 126265. ISSN: 09500618. DOI: 10.1016/j.conbuildmat.2021.126265. URL: https://linkinghub.elsevier.com/retrieve/pii/S0950061821039957 (visited on 03/25/2022).

[54] Zeina Mahayri, George Patrinos, and Bassam R. Ali. "Toxicity and Pharmacogenomic Biomarkers in Breast Cancer Chemotherapy". In: *Frontiers in Pharmacology* 11 (Apr. 2020), p. 445. DOI: 10.3389/fphar.2020.00445.

[55] Tarek Maylaa et al. "An evaluation of computational learning-based methods for the segmentation of nuclei in cervical cancer cells from microscopic images". en. In: *Current Computer-Aided Drug Design* 18 (Feb. 2022). ISSN: 15734099. DOI: 10.2174/1573409918666220208120756. URL: https://www.eurekaselect.com/200924/article (visited on 05/20/2022).

[56] Steve Morgan et al. "The cost of drug development: a systematic review". eng. In: *Health Policy (Amsterdam, Netherlands)* 100.1 (Apr. 2011), pp. 4–17. ISSN: 1872-6054. DOI: 10.1016/j.healthpol.2010.12.002.

[57] Peter Naylor et al. "Nuclei segmentation in histopathology images using deep neural networks". In: *2017 IEEE 14th International Symposium on Biomedical Imaging (ISBI 2017)*. Melbourne, Australia: IEEE, Apr. 2017, pp. 933–936. ISBN: 978-1-5090-1172-8. DOI: 10.1109/ISBI.2017.7950669. URL: http://ieeexplore.ieee.org/document/7950669/ (visited on 09/09/2022).

[58] Upesh Nepal and Hossein Eslamiat. "Comparing YOLOv3, YOLOv4 and YOLOv5 for Autonomous Landing Spot Detection in Faulty UAVs". en. In: *Sensors* 22.2 (Jan. 2022), p. 464. ISSN: 1424-8220. DOI: 10.3390/s22020464. URL: https://www.mdpi.com/1424-8220/22/2/464 (visited on 03/15/2022).

[59] Anthony Nichols. "High content screening as a screening tool in drug discovery". eng. In: *Methods in Molecular Biology (Clifton, N.J.)* 356 (2007), pp. 379–387. ISSN: 1064-3745. DOI: 10.1385/1-59745-217-3:379.

[60] Leonardo Noriega and Beaconside Staordshire St Dg. *Multilayer perceptron tutorial*. 2005.

[61] Thais Mayumi Oshiro, Pedro Santoro Perez, and José Augusto Baranauskas. "How Many Trees in a Random Forest?" In: *Machine Learning and Data Mining in Pattern Recognition*. Ed. by David Hutchison et al. Vol. 7376. Series Title: Lecture Notes in Computer Science. Berlin, Heidelberg: Springer Berlin Heidelberg, 2012, pp. 154–168. ISBN: 978-3-642-31536-7 978-3-642-31537-4. DOI: 10.1007/978-3-642-31537-4_13. URL: http://link.springer.com/10.1007/978-3-642-31537-4_13 (visited on 09/09/2022).

[62] Francesco Pampaloni, Emmanuel G. Reynaud, and Ernst H. K. Stelzer. "The third dimension bridges the gap between cell culture and live tissue". eng. In: *Nature Reviews. Molecular Cell Biology* 8.10 (Oct. 2007), pp. 839–845. ISSN: 1471-0080. DOI: 10.1038/nrm2236.

[63] Olaf Ronneberger, Philipp Fischer, and Thomas Brox. "U-Net: Convolutional Networks for Biomedical Image Segmentation". en. In: *Medical Image Computing and Computer-Assisted Intervention – MICCAI 2015*. Ed. by Nassir Navab et

al. Vol. 9351. Series Title: Lecture Notes in Computer Science. Cham: Springer International Publishing, 2015, pp. 234–241. ISBN: 978-3-319-24573-7 978-3-319-24574-4. DOI: 10.1007/978-3-319-24574-4_28. URL: http://link.springer.com/10.1007/978-3-319-24574-4_28 (visited on 03/10/2022).

[64] Błażej Ruszczycki et al. "Three-Dimensional Segmentation and Reconstruction of Neuronal Nuclei in Confocal Microscopic Images". In: *Frontiers in Neuroanatomy* 13 (Aug. 2019), p. 81. ISSN: 1662-5129. DOI: 10.3389/fnana.2019.00081. URL: https://www.frontiersin.org/article/10.3389/fnana.2019.00081/full (visited on 03/10/2022).

[65] Robert E. Schapire. "Explaining AdaBoost". en. In: *Empirical Inference*. Ed. by Bernhard Schölkopf, Zhiyuan Luo, and Vladimir Vovk. Berlin, Heidelberg: Springer Berlin Heidelberg, 2013, pp. 37–52. ISBN: 978-3-642-41135-9 978-3-642-41136-6. DOI: 10.1007/978-3-642-41136-6_5. URL: http://link.springer.com/10.1007/978-3-642-41136-6_5 (visited on 09/09/2022).

[66] Volker Schirrmacher. "From chemotherapy to biological therapy: A review of novel concepts to reduce the side effects of systemic cancer treatment (Review)". eng. In: *International Journal of Oncology* 54.2 (Feb. 2019), pp. 407–419. ISSN: 1791-2423. DOI: 10.3892/ijo.2018.4661.

[67] Uwe Schmidt et al. "Cell Detection with Star-Convex Polygons". In: *Medical Image Computing and Computer Assisted Intervention – MICCAI 2018*. Ed. by Alejandro F. Frangi et al. Vol. 11071. Series Title: Lecture Notes in Computer Science. Cham: Springer International Publishing, 2018, pp. 265–273. ISBN: 978-3-030-00933-5 978-3-030-00934-2. DOI: 10.1007/978-3-030-00934-2_30. URL: http://link.springer.com/10.1007/978-3-030-00934-2_30 (visited on 03/10/2022).

[68] Nahian Siddique et al. "U-Net and Its Variants for Medical Image Segmentation: A Review of Theory and Applications". In: *IEEE Access* 9 (2021), pp. 82031–82057. ISSN: 2169-3536. DOI: 10.1109/ACCESS.2021.3086020. URL: https://ieeexplore.ieee.org/document/9446143/ (visited on 03/25/2022).

[69] Dina Sikpa et al. "Automated detection and quantification of breast cancer brain metastases in an animal model using democratized machine learning

tools". eng. In: *Scientific Reports* 9.1 (Nov. 2019), p. 17333. ISSN: 2045-2322. DOI: 10.1038/s41598-019-53911-x.

[70] Ravindra Sonavane and Poonam Sonar. "Classification and segmentation of brain tumor using Adaboost classifier". In: *2016 International Conference on Global Trends in Signal Processing, Information Computing and Communication (ICGTSPICC)*. Jalgaon, India: IEEE, Dec. 2016, pp. 396–403. ISBN: 978-1-5090-0467-6. DOI: 10.1109/ICGTSPICC.2016.7955334. URL: http://ieeexplore.ieee.org/document/7955334/ (visited on 09/09/2022).

[71] Russell Stewart, Mykhaylo Andriluka, and Andrew Y. Ng. "End-to-End People Detection in Crowded Scenes". In: *2016 IEEE Conference on Computer Vision and Pattern Recognition (CVPR)*. 2016 IEEE Conference on Computer Vision and Pattern Recognition (CVPR). Las Vegas, NV, USA: IEEE, June 2016, pp. 2325–2333. ISBN: 978-1-4673-8851-1. DOI: 10.1109/CVPR.2016.255. URL: http://ieeexplore.ieee.org/document/7780624/ (visited on 02/10/2023).

[72] Carsen Stringer et al. "Cellpose: a generalist algorithm for cellular segmentation". en. In: *Nature Methods* 18.1 (Jan. 2021), pp. 100–106. ISSN: 1548-7091, 1548-7105. DOI: 10.1038/s41592-020-01018-x. URL: http://www.nature.com/articles/s41592-020-01018-x (visited on 03/10/2022).

[73] Lindsey A. Torre et al. "Global Cancer in Women: Burden and Trends". In: *Cancer Epidemiology, Biomarkers & Prevention* 26.4 (Apr. 2017), pp. 444–457. ISSN: 1055-9965. DOI: 10.1158/1055-9965.EPI-16-0858. URL: https://doi.org/10.1158/1055-9965.EPI-16-0858 (visited on 09/09/2022).

[74] Nicholas J. Tustison and James Gee. "Introducing Dice, Jaccard, and Other Label Overlap Measures To ITK". In: *The Insight Journal* (Dec. 2009). ISSN: 2327-770X. DOI: 10.54294/1vixgg. URL: https://www.insight-journal.org/browse/publication/707 (visited on 09/09/2022).

[75] Gail A. Van Norman. "Drugs, Devices, and the FDA: Part 1: An Overview of Approval Processes for Drugs". eng. In: *JACC. Basic to translational science* 1.3 (Apr. 2016), pp. 170–179. ISSN: 2452-302X. DOI: 10.1016/j.jacbts.2016.03.002.

[76] Eleonora Vitali et al. "Metformin and Everolimus: A Promising Combination for Neuroendocrine Tumors Treatment". en. In: *Cancers* 12.8 (Aug. 2020), p. 2143. ISSN: 2072-6694. DOI: 10.3390/cancers12082143. URL: https://www.mdpi.com/2072-6694/12/8/2143 (visited on 03/25/2022).

[77] Mailinh Vu et al. "Cervical cancer worldwide". en. In: *Current Problems in Cancer*. HPV related Cancers 42.5 (Sept. 2018), pp. 457–465. ISSN: 0147-0272. DOI: 10.1016/j.currproblcancer.2018.06.003. URL: https://www.sciencedirect.com/science/article/pii/S014702721830134X (visited on 09/13/2022).

[78] Steven E Waggoner. "Cervical cancer". en. In: *The Lancet* 361.9376 (June 2003), pp. 2217–2225. ISSN: 0140-6736. DOI: 10.1016/S0140-6736(03)13778-6. URL: https://www.sciencedirect.com/science/article/pii/S0140673603137786 (visited on 09/14/2022).

[79] Si Wen et al. "Comparison of Different Classifiers with Active Learning to Support Quality Control in Nucleus Segmentation in Pathology Images". eng. In: *AMIA Joint Summits on Translational Science proceedings. AMIA Joint Summits on Translational Science* 2017 (2018), pp. 227–236. ISSN: 2153-4063.

[80] World Health Organization. *Cervical cancer*. URL: https://www.who.int/health-topics/cervical-cancer#tab=tab_1 (visited on 03/08/2022).

[81] Olivier J. Wouters, Martin McKee, and Jeroen Luyten. "Estimated Research and Development Investment Needed to Bring a New Medicine to Market, 2009-2018". eng. In: *JAMA* 323.9 (Mar. 2020), pp. 844–853. ISSN: 1538-3598. DOI: 10.1001/jama.2020.1166.

[82] Liming Wu et al. "RCNN-SliceNet: A Slice and Cluster Approach for Nuclei Centroid Detection in Three-Dimensional Fluorescence Microscopy Images". en. In: *2021 IEEE/CVF Conference on Computer Vision and Pattern Recognition Workshops (CVPRW)*. Nashville, TN, USA: IEEE, June 2021, pp. 3750–3760. ISBN: 978-1-66544-899-4. DOI: 10.1109/CVPRW53098.2021.00416. URL: https://ieeexplore.ieee.org/document/9522908/ (visited on 03/25/2022).

[83] Fanxin Xu et al. "TE-YOLOF: Tiny and efficient YOLOF for blood cell detection". en. In: *Biomedical Signal Processing and Control* 73 (Mar. 2022), p. 103416. ISSN: 17468094. DOI: 10.1016/j.bspc.2021.103416. URL: https://linkinghub.elsevier.com/retrieve/pii/S1746809421010132 (visited on 03/10/2022).

[84] Yizong Cheng. "Mean shift, mode seeking, and clustering". en. In: *IEEE Transactions on Pattern Analysis and Machine Intelligence* 17.8 (Aug. 1995), pp. 790–799. ISSN: 01628828. DOI: 10.1109/34.400568. URL: http://ieeexplore.ieee.org/document/400568/ (visited on 05/11/2022).

[85] Youyi Song et al. "A deep learning based framework for accurate segmentation of cervical cytoplasm and nuclei". In: *2014 36th Annual International Conference of the IEEE Engineering in Medicine and Biology Society*. Chicago, IL: IEEE, Aug. 2014, pp. 2903–2906. ISBN: 978-1-4244-7929-0. DOI: 10.1109/EMBC.2014.6944230. URL: http://ieeexplore.ieee.org/document/6944230/ (visited on 09/09/2022).

[86] Wei Zhan et al. "An improved Yolov5 real-time detection method for small objects captured by UAV". en. In: *Soft Computing* 26.1 (Jan. 2022), pp. 361–373. ISSN: 1432-7643, 1433-7479. DOI: 10.1007/s00500-021-06407-8. URL: https://link.springer.com/10.1007/s00500-021-06407-8 (visited on 03/25/2022).